AD-A052 052 MEGATEK CORP SAN DIEGO CALIF*
MINIMUF-3: A SIMPLIFIED HF MUF PREDICTION ALGORITHM.(U)
FEB 78 R B ROSE, J N MARTIN, P H LEVINE
F/G 17/2.1
N00123-75-C-0328
NOSC-TR-196

UNCLASSIFIED

| OF |
AD A052 052

END
DATE FILMED
5-78
DDC

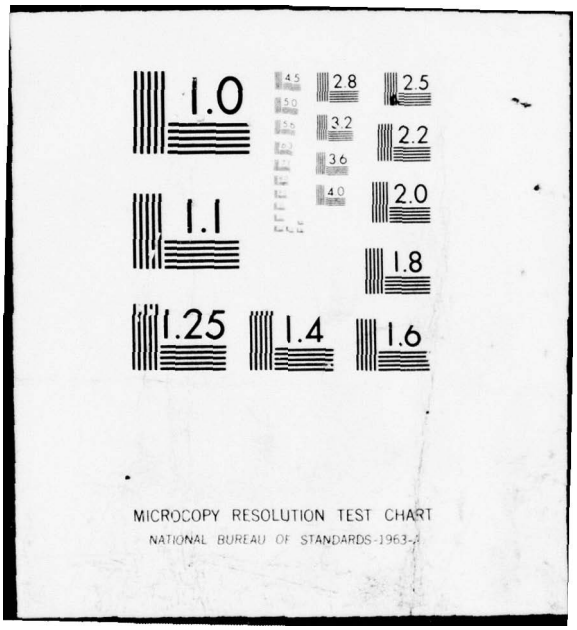
1.0
1.1
1.25
1.4
1.6
1.8
2.0
2.2
2.5
2.8
3.2
3.6
4.0
4.5
5.0
5.6
MICROCOPY RESOLUTION TEST CHART
NATIONAL BUREAU OF STANDARDS-1963-A

(12)

NOSC

NOSC TR 186

NOSC TR 186

Technical Report 186

MINIMUF-3: A SIMPLIFIED hf MUF PREDICTION ALGORITHM

RB Rose and JN Martin
Naval Ocean Systems Center

PH Levine
Megatek Corp

1 February 1978

Final Report: October 1976 — September 1977
Prepared For
Naval Electronic Systems Command (PME-106)

Approved for public release; distribution is unlimited

NAVAL OCEAN SYSTEMS CENTER
SAN DIEGO, CALIFORNIA 92152

NAVAL OCEAN SYSTEMS CENTER, SAN DIEGO, CA 92152

AN ACTIVITY OF THE NAVAL MATERIAL COMMAND

RR GAVAZZI, CAPT, USN
Commander

HL BLOOD
Technical Director

ADMINISTRATIVE INFORMATION

The original MINIMUF model was developed for NOSC by Megatek Corporation under contract N00123-75-C-0328 as part of the SOLRAD-Propagation Forecast (PROPHET) Terminal DT&E (NOSC project MP05) sponsored by the Naval Electronic Systems Command, PME-106. Subsequent refinement, verification, and application development was carried out as part of the CLASSIC PROPHET task (NOSC project MP19) performed for Headquarters, Naval Security Group Command, G-53.

Released by
Dr JH Richter, Head
EM Propagation Division

Under authority of
JD Hightower, Head
Environmental Sciences Department

UNCLASSIFIED

SECURITY CLASSIFICATION OF THIS PAGE *(When Data Entered)*

18 NOSC 19 TR-186

REPORT DOCUMENTATION PAGE

READ INSTRUCTIONS BEFORE COMPLETING FORM

1. REPORT NUMBER: NOSC Technical Report 186 (TR 186)	2. GOVT ACCESSION NO. / 3. RECIPIENT'S CATALOG NUMBER
4. TITLE *(and Subtitle)*: MINIMUF-3: A SIMPLIFIED hf MUF PREDICTION ALGORITHM	5. TYPE OF REPORT & PERIOD COVERED: Final rept Oct 76 – Sep 77
	6. PERFORMING ORG. REPORT NUMBER
7. AUTHOR(s): RB Rose, JN Martin, Naval Ocean Systems Center; PH Levine, Magnetek Corp	8. CONTRACT OR GRANT NUMBER(s): N00123-75-C-0328 new
9. PERFORMING ORGANIZATION NAME AND ADDRESS	10. PROGRAM ELEMENT, PROJECT, TASK AREA & WORK UNIT NUMBERS: NOSC Projects MP05 and MP19
11. CONTROLLING OFFICE NAME AND ADDRESS: NAVELEX PME-106	12. REPORT DATE: 1 February 1978 / 13. NUMBER OF PAGES: 50 (52 p.)
14. MONITORING AGENCY NAME & ADDRESS *(if different from Controlling Office)*	15. SECURITY CLASS. *(of this report)*: Unclassified / 15a. DECLASSIFICATION/DOWNGRADING SCHEDULE

16. DISTRIBUTION STATEMENT *(of this Report)*

Approved for public release; distribution is unlimited

17. DISTRIBUTION STATEMENT *(of the abstract entered in Block 20, if different from Report)*

18. SUPPLEMENTARY NOTES

19. KEY WORDS *(Continue on reverse side if necessary and identify by block number)*

hf Propagation
Propagation forecasting
Maximum usable frequency (MUF)
Solar sunspots
BASIC
FORTRAN

20. ABSTRACT *(Continue on reverse side if necessary and identify by block number)*

MINIMUF-3 is a semiempirical model for predicting the maximum usable frequency (MUF) for hf propagation. It was designed to allow simplified hf propagation predictions to be performed in a near-real-time mobile, tactical environment. An 80-statement BASIC language subroutine is presented which outputs MUF for arbitrary input values of receiver/transmission position, month, date, time (UT), and solar sunspot number. The program is compatible with existing and newly emerging generations of mini- and microprocessor-based computers. Results of extensive tests comparing MINIMUF-3 against hf oblique sounder data are also presented. The sounder data encompassed 196 path months (4704 test points) of observed MOFs from 23 different hf transmission paths. The

DD FORM 1 JAN 73 1473 EDITION OF 1 NOV 65 IS OBSOLETE
S/N 0102-LF-014-6601

391984

UNCLASSIFIED

SECURITY CLASSIFICATION OF THIS PAGE *(When Data Entered)*

20. (Cont) overall rms residual error of MINIMUF-3 was 3.83 MHz. The results compared favorably with those obtained from large-scale hf prediction codes that were exercised against the same sounder data set.

OBJECTIVE

Develop the MINIMUF-3 model to provide a simplified prediction of hf Maximum Usable Frequency (MUF) suitable for use on small mobile propagation forecast (PROPHET) terminals. With this tool, develop a variety of new forecast applications to serve the hf surveillance and communications community where the use of large-scale propagation programs in the operational environment is not practical. (The flexibility of these new applications to serve a variety of users depends to a large extent on the confidence of the internal prediction algorithms. Because MINIMUF-3 represents such a significant degree of simplification, a primary concern is the accuracy of the MUF estimates.) This report presents: (1) the MINIMUF model; (2) results of verification tests; (3) a specification on its capabilities and limitations; and (4) applications.

RESULTS

The MINIMUF-3 hf prediction model produces a consistent product with a nominal accuracy between 3 and 5 MHz rms residual error. This compares favorably with the abilities of large-scale hf prediction programs which require sizable computer facilities.

RECOMMENDATIONS

Continue work to further refine the MINIMUF-3 model to include E and Sporadic E region propagation. Consider small-scale propagation forecast (PROPHET) capabilities for inclusion into new hf system development. Further continue new application development to exploit the capabilities of simple forecast models like MINIMUF-3.

ACKNOWLEDGEMENTS

The development and verification of the MINIMUF-3 model has been a team effort. The authors would like to acknowledge the work of RW Eberhardt of the San Diego State University Foundation in preparing the enormous amount of data used in this study; RW Rose of the Systems Development Corporation in developing the BASIC programs needed to make MINIMUF-3 usable on desk-top graphic calculators; and DB Sailors, who provided consultation on the large-scale hf prediction programs and technical review of this report.

CONTENTS

ILLUSTRATIONS

TABLES

INTRODUCTION

The performance of any system operating in the high-frequency (hf) spectrum between 2 and 32 MHz is subject to certain physical boundaries on the propagation of its signal. These constraints are unique and definable for any given point in time and over any path. The upper boundary is called the maximum usable frequency (MUF). The classical MUF is the highest frequency that can propagate by a particular mode between two points by ionospheric refraction. The standard MUF, as defined by the CCIR (ref 1 and 2), is an approximation to the classical MUF obtained by combining data from vertical ionospheric soundings with a simplified analytical solution of the oblique incidence refraction problem When observing swept frequency oblique incidence sounding data, the upper frequency limit is referred to as the maximum observed frequency (MOF). The MUF (or MOF) is a direct function of ionospheric electron density and is an absolute frequency limit in that the ionosphere is not capable of supporting higher frequencies for that path. The lower boundary is called the lowest usable (or observed) frequency (LUF or LOF). This is a function of absorption occurring during daylight hours and can be correlated directly with solar zenith angle. The band of frequencies between the MUF and LUF is the propagation bandwidth or the spectrum with which the user has to work. The cyclic nature of the propagating bandwidth as it changes from night to day is shown in fig 1 along with the MOF and LOF boundaries. When an hf system operator has prior knowledge of the changes in propagation on the transmission paths he wants to use, he can adjust his frequency selection to remain within the propagating bandwidth. When he has no such knowledge, his operation is vulnerable to these propagation changes.

The SOLRAD-Propagation Forecast (PROPHET) concept (ref 3) is based on providing a near-real-time assessment of the hf propagating bandwidth as a function of time of day, season, solar activity, and transmission path geometry. This is accomplished by combining established and new hf prediction techniques and driving the resulting forecast algorithms with geophysical measurements of those solar emissions which have an impact on propagation parameters. While many of the ideas behind PROPHET have been technically feasible for some time, recent advances in mini- and microcomputer technology have made the use of these concepts also economically feasible. The initial PROPHET concept (described in ref 3) uses prestored tables generated by a standard hf prediction program to calculate MUF on a large computer. Since the terminal can only calculate paths originating or terminating at the location for which the tables have been computed, the MUF algorithm in PROPHET is limited to the fixed paths within the range of the tables and is not adaptable for mobile operation.

---

1. International Radio Consultative Committee, 13th Plenary Assembly, Geneva 1974, Recommendation 373-3; Definitions of Maximum Transmission Frequencies, International Telecommunications Union, 1975

2. Bennington, TW, "How Many MUFs?, Wireless World, v 65, p 537-538, December 1959

3. Richter, Dr JH, IJ Rothmuller and RB Rose, PROPHET: Real Time Propagation Forecasting Terminal, paper presented at 7th Technical Exchange Conference, El Paso, Texas, 30 November 1976.

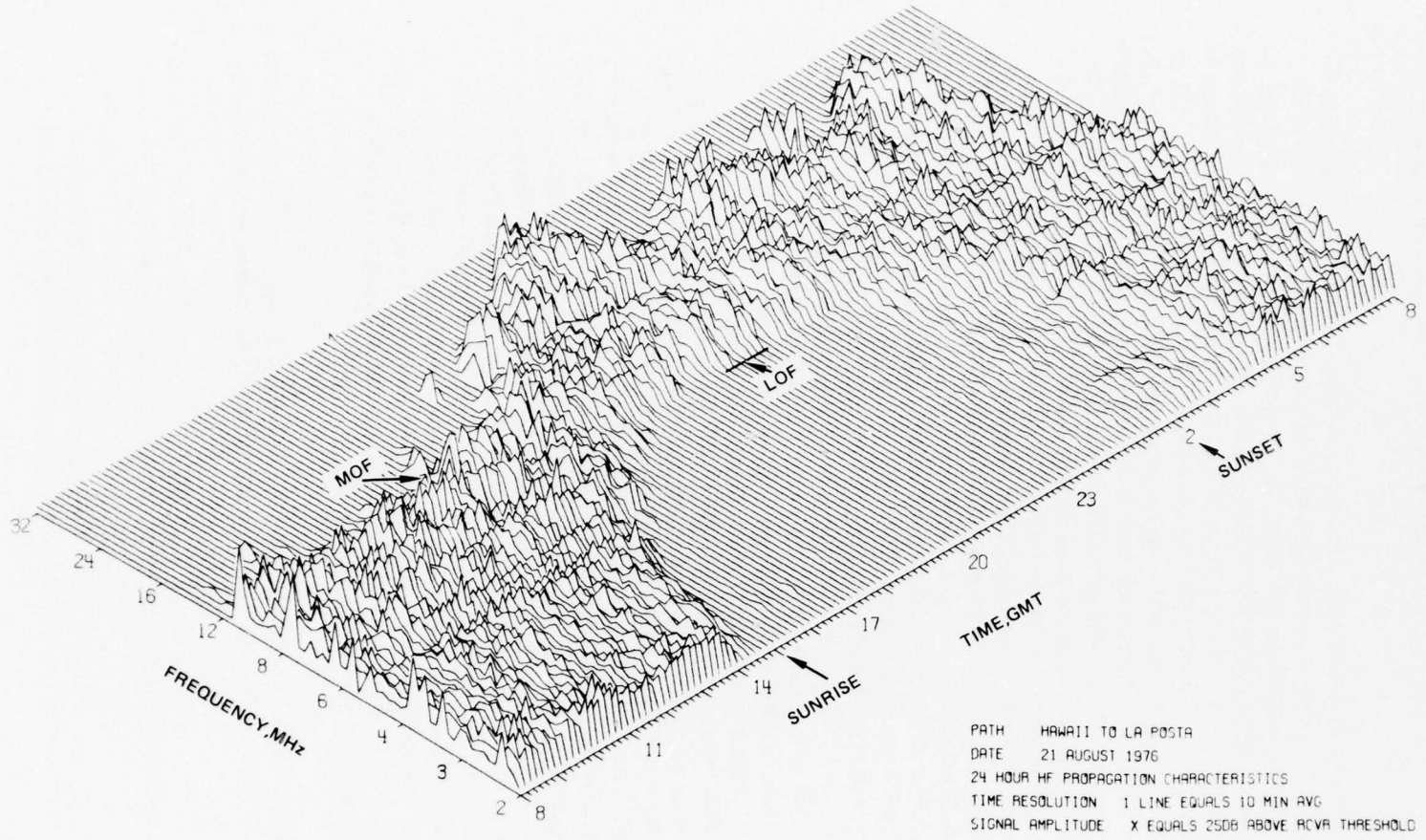

Figure 1. Cyclic nature of propagating bandwidth as it changes from night to day.

New concepts in applying PROPHET to hf signal security, surveillance, and propagation tactics required a more mobile system. To accomplish this, the MUF calculation had to be simplified to the extent that it could be run on new microprocessor-based systems. The MINIMUF model was developed on the premise that the majority of hf predictions needed for the employment of propagation tactics and certain hf surveillance missions need only be first-order approximations, especially in a mobile environment. MINIMUF-3 is the current stage of refinement of the original model.

METHOD OF TESTING

To develop a sufficient knowledge on the capabilities of MINIMUF-3, two verification approaches were considered. The first was to compare MINIMUF-3 against as many swept frequency hf oblique sounder data as could be assembled in a reasonable time. This, in effect, would indicate how the model performs when correlated with "real-world" propagation. The second approach was to compare MINIMUF-3 results against large-scale hf propagation prediction programs such as ITS-78 (Red Deck, ref 4), ITS-78 (Blue Deck, ref 4), and ESSA-ITSA-1 (ref 5), which is the basis for the NAVY standard NTP-6 hf predictions. The latter type of comparison would provide a relative indication of the difference between a first-order approximation and a sophisticated prediction code. While both approaches were considered useful, heavy emphasis was placed on the comparison with oblique sounder data. Since the large-scale programs were considered too expensive to rerun for the project, comparisons with the results of other prediction programs were performed where data already existed.

OBLIQUE SOUNDER DATA BASE PREPARATION

The oblique sounder data base assembled for the MINIMUF-3 verification was derived from a variety of sources and spans the period between 1960 and 1976. This represents more than one complete solar sunspot cycle of propagation data. Attempts were made to make the data base as diverse as possible by including many different path lengths, orientations, and geographical locations.

While measurements from several different types of oblique sounder systems were included, the majority of data came from the Navy Tactical Sounder System (NTSS). To familiarize the reader with oblique sounding principles, a brief description of the NTSS follows.

---

4. Environmental Sciences Services Administration technical report ERL-110-ITS-78, Predicting Long Term Operational Parameters of High Frequency Sky Wave Telecommunication Systems, by AF Barghausen, JW Finney, LL Proctor and LD Schultz, May 1969.

5. Environmental Sciences Services Administration technical report IER-1-ITSA-1 Predicting Statistical Performance Indexes for High Frequency Ionospheric Telecommunication Systems, by DL Lucas, GW Haydon, et al, August 1966

NAVY TACTICAL SOUNDER SYSTEM (NTSS)

The Navy's oblique ionospheric sounder system consists of several shore-based sounder transmitters and a number of sounder receivers. AN/FPT-11 (XN-1) sounder transmitters are installed at selected Naval Communications Stations, research installations, and aboard ships.

AN/FPT-11 Transmitter. Once each minute, the FPT-11 transmitter sequentially transmits a pulse on each of 80 discrete channels between 2 and 32 MHz; the total scan consists of 160 pulses and has a scan time of 16 seconds. The frequency range is divided into four active bands, with 20 channels linearly spaced within each band; the spacing between adjacent channels is doubled, proceeding from one band to the next band. The spacings are 100 kHz in the 2-to-4-MHz range (Band A); 200 kHz in the 4-to-8-MHz range (Band B); 400 kHz in the 8-to-16-MHz range (Band C); and 800 kHz in the 16-to-32-MHz range (Band D). These spacings provide a 5% frequency resolution at the low frequency limit of each band and a 2.5% frequency resolution at the upper frequency limit of each band. Table 1 shows the exact channels used by the FPT-11. Each frequency transmitted consists of two pulses separated by 50 milliseconds. Each 2.6 ms pulse is composed of a series of 13 subpulses, biphase-coded in a Barker-code sequence. The use of Barker coded pulse compression increases the effective transmitter power, retains necessary pulse resolution, and increases the received signal-to-noise ratio by 13:1. To eliminate interference between transmitters, starting times of the 16-second scan are staggered, each transmitter site being assigned a precise time. The transmitter power is normally 30 kW (PEP). The antenna must be wideband, 50- to 72-ohm impedance, and have a VSWR of less than 3:1 over the band of 2 to 32 MHz.

AN/UPR-2 Receiver. The AN/UPR-2 receiver sequentially processes the pulse-train input by starting the gated receiver scan at the time of the transmission. This is accomplished by synchronizing to a common timing source (ie, WWV) and maintaining an accurate time-base generator in the receiver. Signal processing is required since each sounder signal is composed of a series of 13 subpulses; each subpulse compression is such that the signal pulse voltages add arithmetically but the noise does not. The improvement in signal-to-noise ratio (process gain) is the voltage ratio of N:1, where N is the number of RF pulses in the sequence. For the 13-bit code, the process gain is 11 dB. (The Barker code is used because, after processing, it produces a video pulse having a 13:1 peak-to-sidelobe ratio, which was found to be optimum for 13-bit codes.) The resultant or summed pulses are then fed to a storage oscilloscope, which is used to present this pulse information in video form. A storage oscilloscope incorporated in the sounder receiver displays and retains each scan.

Table 1. AN/FPT-11 Step Sounder Frequency Channels (2-32 MHz).

BAND A (MHz)	BAND B (MHz)	BAND C (MHz)	BAND D (MHz)
2.075	4.14	8.3	16.6
2.175	4.35	8.7	17.4
2.275	4.55	9.1	18.2
2.375	4.75	9.5	19.0
2.475	4.95	9.9	19.8
2.575	5.15	10.3	20.6
2.675	5.35	10.7	21.4
2.775	5.55	11.1	22.2
2.875	5.75	11.5	23.0
2.975	5.95	11.9	23.8
3.075	6.15	12.3	24.6
3.175	6.35	12.7	25.4
3.275	6.55	13.1	26.2
3.375	6.75	13.5	27.0
3.475	6.95	13.9	27.8
3.575	7.15	14.3	28.6
3.675	7.35	14.7	29.4
3.775	7.55	15.1	30.2
3.875	7.75	15.5	31.0
3.975	7.95	15.9	31.8

This display, shown in fig 2, indicates which frequencies are propagating [lowest observed frequency (LOF) to maximum observed frequency (MOF)] and which frequencies will be highly distorted because of multipath time delay. An additional data output from the standard UPR-2 is a strip chart record, which is produced concurrently with each ionogram record. These outputs provide a permanent record of the daily variations of the scanned spectrum between 2 and 32 MHz.

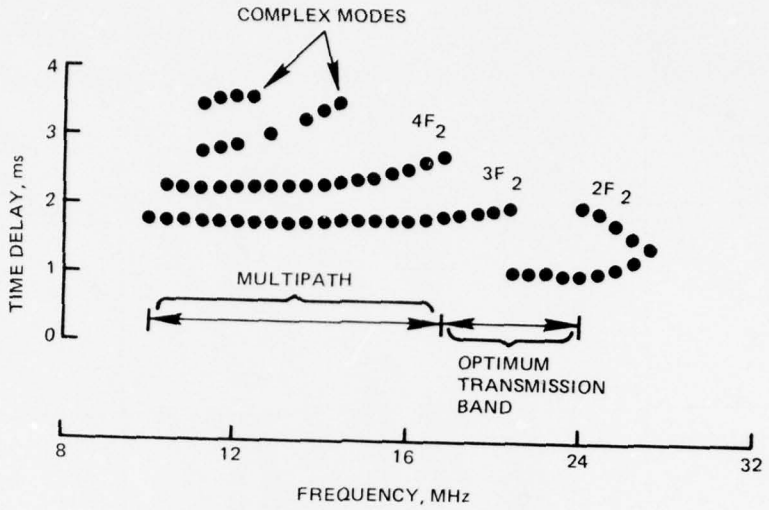

Figure 2. Ionogram of oblique sounder transmission from Naval Communications Station, Hawaii.

Hf Digital Recorder (HFDR). To supplement this capability, NOSC developed a method of digitizing the video output signal and recording it on magnetic tape. This method evolved into the design, construction, and implementation of the hf digital recorder (HFDR) shown in fig 3.

Figure 3. Hf digital recorder (HFDR).

The hf sounder digital data recording system is a self-contained unit consisting of two primary subsystems:

a. The analog to digital (A/D) and timing interface (DIGITIZER); and
b. The magnetic tape transport.

With minor modification to the AN/UPR-2, the HFDR operates concurrently with the AN/UPR-2 receiver and in no way affects normal operation. Hence, with the HFDR-II-equipped sounding receiver, all amplitude, time delay, and frequency information is recorded once every minute, 24 hours a day.

OTHER SOUNDER SYSTEMS

Data collected prior to 1968 were measured on a variety of systems. These included Granger 900 systems, Modified Granger 1900 systems, Modified C3 ionosondes, and specially developed systems. In general, the frequency steps used by the Granger systems are compatible with the NTSS receivers and in some instances data were acquired by means of a Granger transmitter and UPR-2 receiver.

DATA CATEGORIZATION

Because of the variety of measurement systems and recording methods, some common MUF parameter had to be established for the comparison with MINIMUF-3. Since most of the data could be reduced to an hourly mean MUF as a function of month and year (hence sunspot number), the *path-month* was established as the basic data block for comparison purposes. Each path-month consists of 24 hourly mean MUFs for a given transmission path.

The source of the oblique sounder data was also deemed important because it influences the statistical significance of a given path-month. The overall sounder data were categorized into three sources:

a. NTSS-HFDR
b. NTSS-Strip Chart
c. Non-NTSS.

A path-month MUF curve from the NTSS-HFDR system is generally the product of approximately 40000 digitally processed measurements. The resolution of the NTSS-strip chart system limits this to about 2880 hand-scaled data points per path-month. Because the documentation on the non-NTSS Systems was insufficient with respect to data reduction techniques, a path-month is assumed to consist of 30 points per hour or 720 data points. For these reasons, the investigators in this study placed the greatest confidence in the NTSS-HFDR data.

DESCRIPTION OF OVERALL SOUNDER DATA BASE

The final oblique sounder data set consists of 196 path-months (or 16.33 path-years) of mean hourly MUF values derived from 23 different hf transmission paths. The longest path is 7808 km and the shortest path is 802 km. The set contains a cross section of transmission paths including midlatitude, transauroral, transequatorial, all seasons, and all solar sunspot numbers (SSN). No single path represents more than 12% of the total data set. Table 2 summarizes the basis against which the MINIMUF model was compared.

Table 2. Hf Propagation Oblique Sounder Data Base.

	TRANSMISSION PATH	LATITUDE	LONGITUDE	PATH LENGTH	APPROX ORIENTATION	NUMBER OF PATH-MONTH	% OF SAMPLE	YEAR	SSN RANGE	DATA SOURCE	DATA TYPE
(1)	Palo Alto, CA to Fairbanks, Alaska	37.27°N 64.90°N	122.10°W 147.80°W	3503	N-S	1	–	1964	17	Ref 6	Non-NTSS
(2)	Andoya, Norway to Thessoloniki, Greece	69.00°N 40.38°N	015.00°E 022.56°E	3212	N-S	1	1	1964	17	Ref 6	Non-NTSS
(3)	Honolulu, Hawaii to Kodiak, Alaska	21.42°N 57.67°N	158.15°W 152.47°W	4057	N-S	6	3	1969-71	71-104	Ref 7	NTSS (ST)
(4)	Davis, CA to La Posta, CA	38.5°N 32.68°N	121.68°W 116.43°W	802	–	6	3	1971	65-70	NOSC file	NTSS*(ST)
(5)	Toulouse, France to Keflavik, Iceland	43.00°N 63.98°N	002.00°E 022.60°W	2806	–	13	7	1975-76	12-22	NOSC file	NTSS**(HFDR)
(6)	Honolulu, Hawaii to La Posta, CA	21.52°N 32.68°N	158.15°W 116.43°W	4287	–	14	7	1974-76	12-34	NOSC file	NTSS (HFDR)
(7)	Coco-Solo, CZ to Stockbridge, NY	09.37°N 43.00°N	079.88°W 075.50°W	3763	N-S	7	4	1966-67	57-79	Ref 9	Non-NTSS
(8)	Guam to Honolulu, Hawaii	13.47°N 21.52°N	144.8°E 158.15°W	6100	E-W	24	12	1969-71 1974-76	71-104 13-33	Ref 8 NOSC file	NTSS (ST) NTSS (HFDR)
(9)	Andoya, Norway to New Delhi, India	69.00°N 28.60°N	015.00°E 077.20°E	5958	E-W	6	3	1964	10-14	Ref 6	Non-NTSS
(10)	Palo Alto, CA to Thule, Greenland	37.27°N 76.5°N	122.1°W 068.8°W	5069	N-S	2	1	1964	17	Ref 6	Non-NTSS
(11)	Honolulu, Hawaii to Washington, D. C.	21.42°N 38.75°N	158.15°W 76.85°W	7808	–	4	2	1964	17	Ref 8	Non-NTSS
(12)	Tarlac, Philippines to Yokohama, Japan	15.35°N 35.48°N	120.37°E 139.48°E	2936	–	2	1	1968	106-108	Ref 7	NTSS (ST)
(13)	Davis, CA to Honolulu, Hawaii	38.50°N 21.52°N	121.68°W 158.00°W	3938	E-W	4	2	1964	17	Ref 8	Non-NTSS
(14)	Honolulu, Hawaii to Corona, CA	21.42°N 33.86°N	158.15°W 117.55°W	4200	–	22	11	1968-70	87-103	NOSC file	NTSS (ST)

Table 2. (Continued)

TRANSMISSION PATH	LATITUDE	LONGITUDE	PATH LENGTH	APPROX ORIENTATION	NUMBER OF PATH-MONTH	% OF SAMPLE	YEAR	SSN RANGE	DATA SOURCE	DATA TYPE
(15) Guam to Kodiak, Alaska	13.47°N 57.67°N	144.80°E 152.47°W	7139	–	6	3	1969-71	71-104	Ref 7	NTSS (ST)
(16) Toulouse, France to Neimakri, Greece	43.00°N 38.10°N	002.00°E 023.90°E	1922	E-W	4	2	1974-76	14-27	NOSC file	NTSS**(HFDR)
(17) Fort Monmouth, NJ to Palo Alto, CA	40.19°N 37.27°N	074.04°W 122.10°W	4130	E-W	6	3	1961-63	18-65	Ref 10	Non-NTSS
(18) Boulder, Colorado to Barrow, Alaska	40.00°N 71.1°N	105.3°W 156.8°W	4481	–	3	2	1960	120-130	Ref 11	Non-NTSS
(19) Honolulu, Hawaii to Yokohama, Japan	21.42°N 35.48°W	158.15°W	6193	–	8	4	1968 1974-76	105-108 13-34	Ref 7 NOSC file	NTSS (ST) NTSS (HFDR)
(20) Tarlac, Philippines to HEH, Australia	15.35°N 22.33°S	120.37°E 114.15°E	4244	N-S	16	8	1968-69	99-108	Ref 7	NTSS (ST)
(21) Guam to Harold E. Holt, Australia	13.47°N 22.33°S	144.80°E 114.15°E	5196	–	18	9	1968-71	71-108	NOSC file	NTSS (ST)
(22) Davis, CA to Kodiak, Alaska	38.50°N 57.67°N	121.68°W 152.47°W	3111	–	10	5	1969	99-102	Ref 7	NTSS*(ST)
(23) Guam to Yokohama, Japan	13.47°N 38.48°N	144.80°E 139.48°E	2504	N-S	13	7	1968-71 1974-76	71-106 12-34	Ref 7 NOSC file	NTSS (ST) NTSS (HFDR)

*Granger (900) xmtr, UPR-2 rcvr (strip chart).

**French xmtr FPT-11 equivalent.

6. Stanford Research Institute, technical summary report no. 7, Long Range Propagation Experiment, ONR contract no 3853(00), ARPA order 196-62 November 1964.

7. Chief of Naval Operations (OEG) letter report, Data for Comparison of Ionospheric Sounder Measurements with Predicted Optimum Frequencies for Communication Circuits, letter serial (OEG) 154-70, 12 March 1970.

8. Booz, Allen, An Examination of the Data Presently Available for the Development of a Short-term Warning Capability, Applied Research Inc, report 800-9-5, prepared under contract no 93296, project serial no SS-267-001, task 7645, 23 February 1966.

9. General Electric Co, Expanded Little Ida, Experimental Results, technical report no RADC-TR-67-618, prepared under contract AF30(602)-3946 for Rome Air Development Center, December 1967.

10. Stanford Research Institute, interim technical report 4, HF Communications Effects Simulation: Comparison of the Fort Monmouth/Palo Alto Circuit Performance with Computer Predictions, Army contract DA-36-039, SC-87197, DASA subtask 938/04-014, January 1964.

11. US Department of Commerce, Boulder–Barrow Sweep Frequency Oblique Pulse Experiment, NBS report 7217 by LH Tveten, 8 January 1962.

While sounder MUF data were available in the NOSC data file, it was believed that the paths listed in table 2 represented a sufficient cross section of propagation conditions to test MINIMUF-3 thoroughly.

Because the data came from a variety of sources, a standard format was established and a master data tape was constructed listing the hourly (UT) mean MUFs and all pertinent path parameters.* Once constructed, the desired comparisons to the MINIMUF-3 model were a relatively straightforward process using the NOSC SEL810B computer system.

* A copy of this tape can be made available upon request through Commander, NOSC.

MINIMUF MODEL DEVELOPMENT

THEORETICAL BACKGROUND

A central task of long-term statistical hf propagation forecasting is the prediction of maximum usable frequency (MUF). The MUF, in turn, is principally controlled by the critical frequency of the F_2 layer of the ionosphere, f_oF_2, and it is the success in predicting this quantity that primarily determines the accuracy of the MUF forecast. Unlike the E and F_1 layers, which can be modeled quite well as a function of a single parameter—cos χ (the cosine of the instantaneous solar zenith angle) proportional to the solar intensity—the physics of the F_2 layer is generally believed to involve an interaction of photochemical and transport processes sufficiently complex that diurnal, seasonal, and geographical f_oF_2 variations cannot be simply accommodated through the corresponding variations in cos χ. Indeed, one even speaks of F_2 layer "anomalies" when comparing observed f_oF_2 with expectations based on the instantaneous cos χ (ref 12 and 13). For example, f_oF_2 can be higher at midday in winter than in summer ("seasonal" anomaly), and on a given day can peak in late afternoon rather than at midday ("diurnal" anomaly).

Therefore, while f_oF_2 cannot be modeled as a function of the instantaneous cos χ, the possibility remains that it could be modeled as the response of a dynamic system "driven" by a function of cos χ. Examination of the shape of observed f_oF_2 diurnal profiles, for example, suggests that a simple relaxation model, according to which f_oF_2 represents a lagged response to the instantaneous solar intensity, may be useful as a first approximation. Allowing the lag time constant to be long ($\sim$ 10 hours) in summer and short ($\sim$ 1 hour) in winter at middle and equatorial latitudes could then at least partially reproduce both the seasonal and diurnal anomalies.

Accordingly, a semiempirical model for f_oF_2 has been developed based on the analogy to a single-lag linear system (eg, an RC circuit) driven by a forcing function proportional to the instantaneous cos χ. Further simplifying assumptions of the model are as follows:

1. The lag time constant during the day is a simple monotonic function of the midday solar zenith angle.
2. The time constant at night is a constant (2 hours) independent of season or geographical location.

As with other semiempirical models of complex geophysical processes, no attempt is made to justify the model in terms of the underlying physical mechanisms. Rather, the model serves to provide a mathematical framework for force-fitting to empirical data. Of course, if the model is successful in fitting a large data base with reasonable accuracy and relatively few adjustable constants, the physical reality of the assumed relaxation process gains credibility and may guide the understanding of the underlying mechanisms.

---

12 JA Ratcliffe and K Weekes, in Physics of the Upper Atmosphere, JA Ratcliffe (ed), p 427–432, Academic Press, New York, 1960.

13 Rishbeth, H, A review of Ionospheric F Region Theory, Proc IEEE, v 55, p 16–35, January 1967.

A key feature of the proposed f_oF_2 model is that seasonal and geographical variations of the predicted f_oF_2 arise only from the corresponding variations in the midday solar zenith angle, in marked contrast to the customary procedure of numerically mapping f_oF_2 by fitting appropriate mathematical functions to observed ionospheric sounding data collected from a worldwide net of vertical sounders (ref 14, 15, and 16). Furthermore, by making simple analytical approximations to the dynamic solutions of the model (ie, the diurnal response function), we end up with a simple closed-form expression for f_oF_2 as a function of midday solar zenith angle, sunspot number, and time relative to local sunrise and sunset. By appending simple approximations for the M factor (ie, MUF/f_oF_2) and for solar zenith angle as a function of location and time, we arrive at a model for MUF which is sufficiently compact to be coded for computation on a minicomputer or desktop programmable scientific calculator.

MATHEMATICAL MODELS

f_oF_2

Let $\cos\chi$ be the cosine of the actual instantaneous solar zenith angle at an ionospheric height representative of the F_2 layer, and let $\cos\chi_{eff}$ be the "effective" value of this quantity taking relaxation processes into account. The basic assumed form for f_oF_2 is

$$f_oF_2 = \left(1+R/R_o\right)\sqrt{A_o+A_1\left(\sqrt{\cos\chi_{eff}}\right)} \tag{1}$$

where R = sunspot number and R_o, A_o, and A_1 are constants independent of geographic location and time*. To model $\cos\chi_{eff}$, we begin by constructing the quantity:

$$\left(\cos\chi_{eff}\right)_{NIGHT} = \left(\cos\chi_{eff}\right)_{SUNSET} \cdot \exp\left[-\left(T - T_{SUNSET}\right)/\tau_N\right] \tag{2}$$

---

14 International Radio Consultative Committee, Oslo, 1966, Report 340; CCIR Atlas of Ionospheric Characteristics, International Telecommunications Union, Geneva, 1975.

15 International Radio Consultative Committee, New Delhi, 1974, Supplement No 1 to Report 340; CCIR Atlas of Ionospheric Characteristics, International Telecommunications Union, Geneva, 1971.

16 International Radio Consultative Committee, Geneva, 1974, Supplement No 2 to Report 340; CCIR Atlas of Ionospheric Characteristics, International Telecommunications Union, Geneva, 1975.

* This form was motivated by the following physical considerations: (1) at the peak of a Chapman layer, the solar-induced electron production rate is $\alpha\cos\chi$; (2) assuming the net effect of the electron-loss chemistry to be recombinationlike, the solar-induced increase in electron density over ambient is α(production rate)$^{1/2}$; (3) for a collisionless plasma, critical frequency is α(electron density)$^{1/2}$.

In equation 2, τ_N is a nighttime relaxation time which is taken to be a constant independent of season and geographical location. $T - T_{SUNSET}$ is the elapsed time in hours since sunset.

During the day, a different relaxation time, τ_D, is assumed. In contrast to τ_N, τ_D is markedly dependent on location and position, albeit in an analytically simple fashion. Specifically, we assume the daytime relaxation time to be a function of the actual noon-time solar zenith angle ($\cos \chi_{NOON}$):

$$\tau_D = \tau_o \left(\cos \chi_{NOON}\right)^{P_2} \tag{3}$$

where τ_o and P_2 are again constants independent of season or location. Note that during summer at equatorial and moderate latitudes, $\tau_D \rightarrow \tau_o$, whereas in the winter $\tau_D << \tau_o$.

The time dependence of $\cos \chi_{eff}$ during the day is approximated as follows. First, we simplify the time dependence of the actual $\cos \chi$ in terms of its value at noon, $\cos \chi_{NOON}$, as:

$$\cos \chi \approx \cos \chi_{NOON} \cdot \sin \left[\frac{\pi (T-T_{DAWN})}{\Delta T} \right] \tag{4}$$

where ΔT is the daytime duration given by

$$\Delta T = T_{SUNSET} - T_{DAWN} \tag{5}$$

and noon occurs when $T = T_{DAWN} + \Delta T/2$. Next, $\cos \chi_{eff}$ is assumed to represent the response of a linear first-order system "driven" by the actual $\cos \chi$:

$$\tau_D \frac{d}{dt} (\cos \chi_{eff}) + \cos \chi_{eff} = \cos \chi. \tag{6}$$

Using equation 4 for the right hand side of equation 6 and integrating, we obtain for the daytime $\cos \chi_{eff}$:

$$\left(\cos \chi_{eff} \right)_{DAY} = \frac{\cos \chi_{NOON}}{1 + \beta^2} \left\{ \sin \alpha + \beta \left(\exp \left[- \frac{(T-T_{DAWN})}{\tau_D} \right] - \cos \alpha \right) \right\} \tag{7}$$

where

$$\beta = \frac{\pi \tau_D}{\Delta T} \tag{8}$$

and

$$\alpha = \frac{\pi(T-T_{DAWN})}{\Delta T} \quad . \tag{9}$$

Evaluating equation 7 at sunset ($T-T_{DAWN} = \Delta T$), we find

$$\left(\cos \chi_{eff}\right)_{SUNSET} = \frac{\cos \chi_{NOON}}{1+\beta^2} \left\{ \beta \left[1 + \exp\left(\frac{-\Delta T}{\tau_D} \right) \right] \right\} \tag{10}$$

which completes the specification of f_0F_2 at night via equations 1 and 2.

Finally, to avoid unphysical discontinuities in $\cos \chi_{eff}$ just after sunrise, we do not allow $\cos \chi_{eff\ DAY}$ to fall below its value just prior to sunrise as computed from equation 2. Thus we impose the condition

$$\left(\cos \chi_{eff}\right)_{DAY} = MAX \left\{ \left(\cos \chi_{eff}\right)_{SUNSET} \cdot \exp\left[(\Delta T-24)/\tau_N \right] , \left(\cos \chi_{eff}\right)_{DAY\ (eq\ 7)} \right\} \tag{11}$$

The basic f_0F_2 model is therefore given in equations 1, 2, and 10 for nighttime (ie, $T_{SUNSET} < T < T_{DAWN}$) and equations 1, 7, and 11 for daytime ($T_{DAWN} < T < T_{SUNSET}$).

EQUATION OF TIME

In this section, we present simple analytical approximations for the times of local noon, sunrise, and sunset, and for the noon value of the solar zenith angle. To an acceptable degree of accuracy, we find for the Universal Time of local noon the approximation:

$$T_{NOON} = \frac{W}{15^\circ} + 12 + 0.13 \left[\sin Y_1 + 1.2 \sin (2Y_1) \right] \bmod (24) \tag{12}$$

where

W = longitude west of Greenwich [0, 360°]

Y_1 = 0.0172 (D+10)

D = 30.4 (M1-1) + D1

D1 = day [1, 31]

M1 = month [1,12].

In terms of the subsidiary variable y_2 defined by

$$y_2 = 0.409 \cos Y_1 \quad \text{[radians]} \tag{13}$$

and L = north latitude in degrees [-90, 90]

we have

$$\cos \chi_{NOON} = \left[\cos \frac{\pi}{2} \left(\frac{L}{90^\circ} \right) + y_2 \right] \tag{14}$$

The duration of the daytime, ΔT, is approximated by

$$\Delta T = \frac{24}{\pi} \text{ arc cos } \left(\frac{-0.26 + \sin y_2 \sin L}{\cos y_2 \cos L} \right) \quad \text{[hours]} \tag{15}$$

where the factor -0.26 approximately represents the difference between sunrise (or sunset) at the surface of the earth and at F_2 layer heights. From equation 15 there follows

$$T_{DAWN} = T_{NOON} - \Delta T/2 \qquad \text{mod (24)} \tag{16}$$

$$T_{SUNSET} = T_{NOON} + \Delta T/2 \qquad \text{mod (24)}$$

where T_{NOON} is given in equation 12.

CONTROL POINTS

The equations of the foregoing sections yield f_oF_2 at a specified (north) latitude, L, and (west) longitude, W. In an actual application, the latitude and longitude of the receiver and transmitter are given quantities and L and W are to be evaluated at specific "control points" along the great circle propagation path.

From spherical trigonometry, one obtains the following expressions for the great circle arc length, ψ (in radians), connecting two points defined by the (latitude, longitude) pairs (L_1,W_1) and (L_2,W_2):

$$\psi = \text{arc cos} \left[\sin L_1 \sin L_2 + \cos L_1 \cos L_2 \cos (W_2-W_1) \right]. \tag{17}$$

If one travels a fraction, K, of the distance from point 1 to point 2, the north latitude, L_K, and west longitude, W_K, of this location are determined from

$$L_K = \text{arc sin} \left\{ \frac{\sin \left[\psi(1-K) \right] \sin L_1 + \sin (\psi K) \sin L_2}{\sin \psi} \right\} \tag{18}$$

and

$$W_K = \arccos \left\{ \frac{\cos L_1 \cos W_1 \sin \left[\psi(1-K) \right] + \cos L_2 \cos W_2 \sin (\psi K)}{\cos L_K \sin \psi} \right\} . \quad (19)$$

The control point locations are determined in accordance with conventional MUF estimation procedures. Thus if the range, D, from transmitter to receiver is less than 4000 km, the control point is at midpath (K=½). If D ⩾ 4000 km, two control points are considered, respectively located 2000 km in from either terminus.* In this latter case, the procedure we adopt is to compute a MUF for each of two fictitious single-hop paths of length D/2, whose midpaths lie at the control points just defined. The MUF for the actual total path is then taken as the lesser of the two single-hop MUFs. Thus for any D, the problem reduces to the estimation of MUFs for a single-hop path.

M FACTOR

Again following conventional procedure, the MUF for any single-hop path is written as the product:

$$MUF = (f_0F_2)_{\text{mid-path}} \cdot M \quad (20)$$

where the so-called "M factor" is a function of pathlength and layer structure—particularly the height of the layer maximum. In the present model, $(f_0F_2)_{\text{mid-path}}$ is computed at a control point as fully described above. We therefore burden M with accommodating the important "real-world" complexities of hf propagation which have been glossed over in the extremely simple models we have adopted for f_0F_2.

Consider a single-hop path of great-circle arc length ψ (radians) whose midpoint lies at latitude L_0, and whose termini lie at latitudes L_1 and L_2. Let the duration of daylight at midpath be ΔT hours. We approximate the M factor in the following form

$$M = \left\{ 1+2.5[\sin(2.5\psi)]^{3/2} \right\} \cdot G_1(\Delta T) \cdot G_2(L_0) \cdot G_3(L_1, L_2). \quad (21)$$

The first factor of equation 21 embodies the range-dependence of the M factor and was obtained by curve-fitting to exact results for a parabolic layer of 290-km height, with a ratio of semithickness/base height = 0.4. The G_1 factor gives recognition to the ∼50% increase in F_2 layer heights observed at high (northern) latitudes during the summer; ie, at or near "midnight sun" conditions. We specifically choose

$$G_1 = 1 - 0.1 \exp [(\Delta T - 24)/3] \quad (22)$$

which has the effect of a 10% reduction in MUF under full midnight sun conditions, with G_1 recovering rapidly ∼1 as the (midpath) latitude moves toward the equator.

* 1 km = 0.6 statute mile or 0.5 nautical mile.

G_2 is designed to produce further, seasonally independent, reductions in MUF for high-latitude paths. Since propagation data point to fairly abrupt onset of this reduction for | latitudes | $\geq 45°$, we choose the step form:

$$G_2 = \begin{cases} 1 \text{ if } |\text{latitude}| < 45° \\ 0.8 \text{ if } |\text{latitude}| \geq 45° \end{cases} \tag{23}$$

ie, a 20% MUF reduction.

Finally, G_3 is a correction factor for transequatorial paths to take approximate account of the well-known MUF increases on such paths. Applying another 20% correction in step-wise form:

$$G_3 = \begin{cases} 1 \text{ if } L_1, L_2 \text{ of same sign} \\ 1.2 \text{ if } L_1, L_2 \text{ of opposite sign} \end{cases} \tag{24}$$

FIT TO OBLIQUE SOUNDER DATA

The as yet unspecified constants R_o, A_o, A_1 (eq 1); τ_N (eq 2); and τ_o, P_2 (eq 3); together with the correction factors G_1, G_2 and G_3, were determined by iteratively adjusting the model to portions of the data base described earlier. The specific procedure followed was to first identify a limited subset spanning the range of path types (ie, long and short paths, high and moderate latitudes, north-south and east-west, etc). Then for this set, representative path months were chosen and the observed diurnal MUF variations were simultaneously displayed on a high-resolution CRT, using a minicomputer-based Megatek graphics display system. The model was implemented in BASIC in the minicomputer so that direct simultaneous visual comparisons could be made for the whole subset (36 path months) between the observed and predicted diurnal MUF variations. Since computation and display of the 864 MUFs (ie, 36 path months × 24 hours) took about 10 minutes, interactive "tuning" of the model was quite feasible and efficient.

The final parameter values obtained in this way are

R_o = 250 (SSN)
A_o = 6 ($MHz^{1/2}$)
A_1 = 58 ($MHz^{1/2}$)
τ_N = 2 (h)
τ_o = 9.7 (h)
P_2 = 9.6 (exponent—no dimensions).

It is evident from the "roundness" of these numbers that further fine-tuning of the model on an extended data base is still possible. For the present verification purposes, the model was frozen at these parameter values and was designated MINIMUF-3. BASIC and FORTRAN versions are given in the appendices.

MINIMUF-3 VERIFICATION RESULTS

This section will present the results of the MINIMUF-3 verification tests. The objective is to provide the reader with a clear understanding of the capabilities and limitations of the new MUF prediction model.

COMPARISON CRITERIA

The primary comparison parameter used throughout the verification test was RMS error (E_{rms}) between observed oblique sounder MOFs and MUFs calculated by MINIMUF-3. This was calculated by

$$E_{rms} = \left[\frac{1}{n} \sum (m_o - m_c)^2 \right]^{1/2}$$

where m_o = observed hourly mean MUF for a given path month

m_c = calculated MUF for that hour, path, midmonth day, and SSN

n = number of data compared.

The rms error was used because it would show the ability of MINIMUF-3 to track MUF variations along with providing error bounds. In addition, the use of rms error would allow direct comparison of results to previous studies where large-scale hf prediction programs were compared to some of the same hf oblique sounder data used.

The principal method used to assess the accuracy of MINIMUF-3 was to derive the rms error for each path month in the overall data base and assemble these in a variety of categories to determine the strengths and weakness of the model. These comparisons are presented in the following section.

RESULTS OF MINIMUF-3 VERSUS SOUNDER DATA COMPARISON

1. ALL CASES

The oblique sounder data base consisted of 196 path months (16.3 path years) of observed MUFs taken over 23 different hf transmission paths. The shortest path was 802 km and the longest was 7808 km.* Table 3 lists each of the paths and the total rms error for that path.

For the entire 196 path months (4704 hourly points), the overall rms error of MINIMUF-3 was 3.83 MHz. Within this error, the accuracy of 61% of the sample was equal to better than the design goal of 4.0 MHz. The remaining 39% of the tests produced rms errors between 4.05 and 5.82 MHz.

---

* 1 km = 0.6 statute mile or 0.5 nautical mile.

Table 3. MINIMUF-3 rms Error by Sounder Path
(Total Sample = 196 Path months of Data)

No.	Transmission Path	Type Path	Length, km **	Solar Sunspot No	% of Sample	MINIMUF-3 rms Error, MHz
1	Palo Alto, CA, to Fairbanks, Alaska	H, N/S	3503	17	1	2.03
2	Andoya, Norway, to Thessoloniki, Greece	H, N/S	3214	17	1	2.37
3	Honolulu, Hawaii, to Kodiak, Alaska	M, N/S	4057	85	3	2.44
4	Davis, CA, to La Posta, CA	M, N/S	802	67	3	2.46
5	Toulouse, France, to Keflavik, Iceland*	H, N/S	2806	17	7	2.47
6	Honolulu, Hawaii to La Posta, CA*	M, E/W	4287	20	7	2.70
7	Coco Solo, Canal Zone to Stockbridge, NY	LO, N/S	3764	65	4	2.80
8	Guam to Honolulu, Hawaii*	LO, E/W	6100	85, 20	12	3.01
9	Andoya, Norway, to New Delhi, India	M, E/W	5958	12	3	3.12
10	Palo Alto, CA, to Thule, Greenland	TA, N/S	5068	17	1	3.18
11	Honolulu, Hawaii, to Washington DC	M, E/W	7808	17	2	3.41
12	Tarlac, Philippines, to Yokohama, Japan	LO, E/W	2937	107	1	3.56
13	Davis, CA, to Honolulu, Hawaii	M, E/W	3938	17	2	3.58
14	Honolulu, Hawaii, to Corona, CA	M, E/W	4200	95	11	3.63
15	Guam to Kodiak, Alaska	M, N/S	7139	85	3	3.80
16	Toulouse, France, to Neimakri, Greece	M, E/W	1922	20	2	4.05
17	Ft Monmouth, NJ, to Palo Alto, CA	M, E/W	4130	35	3	4.06
18	Boulder, CO, to Pt Barrow, Alaska	H, N/S	481	125	2	4.29
19	Honolulu, Hawaii, to Yokohama, Japan	M, E/W	6193	160, 20	4	4.32
20	Tarlac, Philippines, to HEH, Austrailia	TE, N/S	4244	100	8	4.45
21	Guam to HEH, Australia	TE	5196	85	9	4.50
22	Davis, CA, to Kodiak, Alaska	M, N/S	3112	100	5	5.17
23	Guam to Yokohama, Japan	M, N/S	2505	85, 20	6	5.82

Type of path based on location of control points

M = Midlatitude
E/W = East, west
N/S = North, south
TE = Transequatorial
LO = Low latitude
H = High latitude
TA = Transauroral

All cases rms error = 3.83 MHz

* The data originally used empirically to derive the MINIMUF model.

** 1 km = 0.6213712 statute mile or 0.5399568 nautical mile.

Fully 39.5% of the tests produced an error of less than 3.0 MHz, which is quite encouraging considering the variability of day-to-day MUFs and the makeup of the data in this set (paths 1–8).

Figure 4 shows distribution of rms error for the 196 path months of data. This histogram shows that the overall accuracy characteristics of MINIMUF-3 are centered within the desired range of 1.5–4.0 MHz. Considering all the variables influencing the MUF, the distribution curve is quite well behaved.

** ALL CASES **

CLASS	RMS	FREQ	% FREQ
1	0.5-0.99	1	0.5
2	1-1.49	7	4.0
3	1.5-1.99	16	8.0
4	2-2.49	31	16.0
5	2.5-2.99	22	11.0
6	3-3.49	29	15.0
7	3.5-3.99	32	16.0
8	4-4.49	19	10.0
9	4.5-4.99	11	6.0
10	5-5.49	10	5.0
11	5.5-5.99	6	3.0
12	6-6.49	5	2.5
13	6.5-6.99	1	0.5
14	7-7.49	4	2.0
15	7.5-7.99	1	0.5
16	8-8.49	0	0.0
17	8.5-8.99	0	0.0
18	9-9.49	0	0.0
19	9.5-9.99	0	0.0
20	10-10.49	0	0.0
21	10.5-10.99	0	0.0
22	11.0-11.49	1	0.5

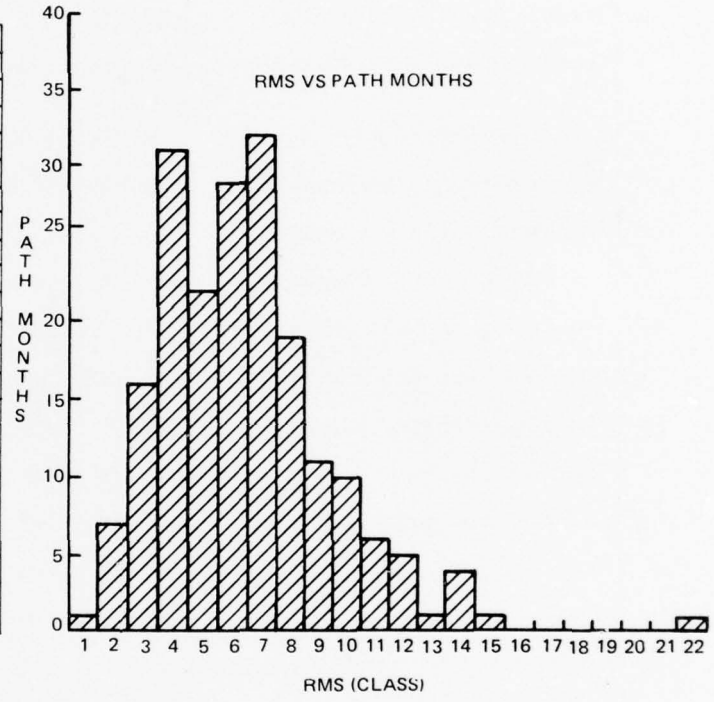

Figure 4. Distribution of rms error by number of path months.

2. DATA TYPE

A critical part of any investigation involving the use of observed measurements is the quality and time resolution of the measurements. This is particularly important when multiple samples are merged into mean values, as was the case with the oblique sounder data. As discussed in the section on data preparation, there were three types of sounder data used: (1) NTSS-HFDR; (2) NTSS-stripchart; and (3) non-NTSS. To determine whether data quality had any impact on the overall accuracy results, table 4 was prepared showing rms error as a function of sounder measurement method.

Table 4. MINIMUF-3 rms error versus sounder data type.

Measurement Method	Sample, path months	% of Sample	rms Error, MHz
NTSS-HFDR	59	30	3.31
NTSS-Stripchart	101	52	4.37
Non-NTSS	36	18	3.27

As would be expected, MINIMUF-3 provides better results when compared to better quality data. The digital NTSS-HFDR System is automatic and can be processed digitally. In general, the sounder instrumentation is of good quality, and care was exercised to maintain the accuracy of the system. A path hour mean MUF for one month from this data is a result of 1800 observations. While the sounding instrumentation of the NTSS-stripchart System was of good quality, the collection and reduction of data were loosely controlled. In general, this type of data collection was an adjunct to normal daily operations at a Navy Communication Station and was not monitored with respect to a specific investigation.

The non-NTSS data were usually project-related. While the instrumentation was of lesser quality than that employed with the NTSS, the close control of the project investigator generally assured its validity. In general, table 4 reflects this differentiation.

3. PATH LENGTH

Figure 5 shows the distribution of MINIMUF-3 rms error as a function of path length. Between ranges of 1000 and 8000 km, the rms error varies around the desired 4.0–MHz accuracy goal, ranging from an error of 4.41 MHz at 2000 km to 3.38 MHz at 6000 km. While fig 5 indicates that there are no drastic range dependencies in MINIMUF-3, the model appears to improve in accuracy with range. This is probably because there are fewer likely modes of propagation at long ranges and the MINIMUF mode selection logic is more apt to be right.

4. PATH ORIENTATION

Table 5 summarizes the performance of MINIMUF-3 as a function of orientation. This categorization is important to assure that the sunrise/sunset reactions are correct for varying degrees of path illumination. The north-south (N-S) paths are those which lie within ±15° of a 0° or 180° bearing. The east-west (E-W) paths are those which fall within ±15° of a 90° or 270° bearing. The paths which did not meet either criterion were put in the "other" category.

Table 5 indicates that MINIMUF-3 is slightly more accurate in predicting E-W paths than N-S paths. This is not surprising, considering the dynamics of the abrupt F-region changes which occur when the entire path is illuminated suddenly, as on N-S paths. However, the magnitude of the error is small enough to assume that MINIMUF-3 will produce consistent results irrespective of path orientation.

** ALL CASES **

LENGTH	FREQ	% FREQ	RMS
L < 1000	6	3	2.46
1000 < L < 2000	4	2	4.05
2000 < L < 3000	28	14	4.41
3000 < L < 4000	23	12	4.08
4000 < L < 5000	67	34	3.66
5000 < L < 6000	26	13	4.13
6000 < L < 7000	32	16	3.38
7000 < L < 8000	10	5	3.65

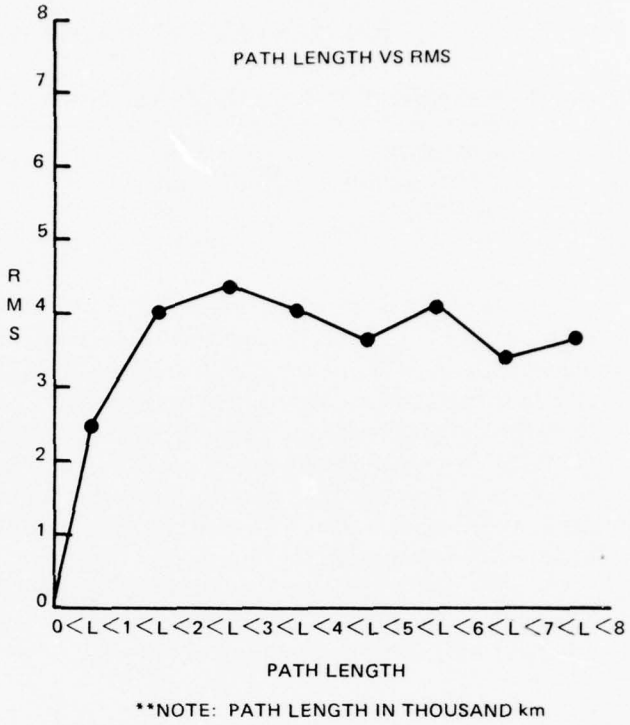

Figure 5. MINIMUF - 3 Rms error as a function of path length.

Table 5. MINIMUF-3 rms error versus path orientation.

Path Orientation	Sample, Path Months	% of Sample	rms Error, MHz
North/south	46	24	4.37
East/west	44	22	3.34
Other	106	54	3.76

5. SEASON/MONTH

Figure 6 shows the distribution of rms error as a function of season and month. MINIMUF-3 is seen to be slightly more accurate in the winter and summer than during the spring and fall. The monthly histogram in fig 6 shows a double error peak at or just after the equinoxes. The month of October was consistently the most difficult to predict for throughout the data set, which was probably a reflection of the complexity of the underlying physical processes.

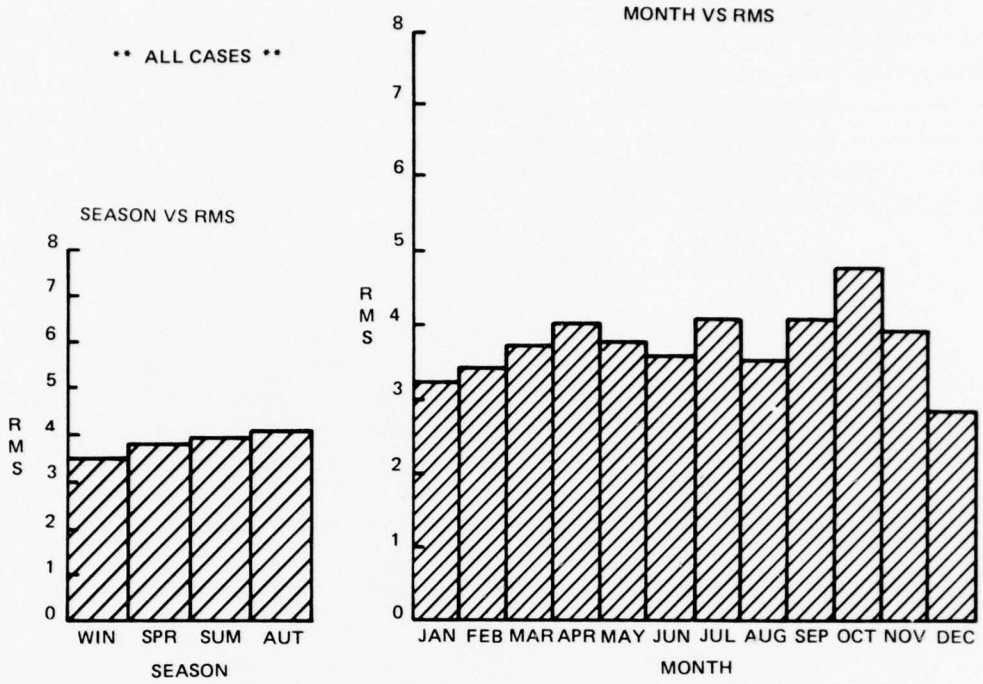

Figure 6. MINIMUF - 3 Rms error as a function of season and month.

6. GEOMAGNETIC LATITUDE

The next tests were made to determine error as a function of geomagnetic latitude. The three categories denote transequatorial propagation, midlatitude propagation, and transpolar propagation. These general areas have entirely different propagation characteristics and problems. Of the three, the midlatitude case should be the best behaved and the most predictable. Table 6 indicates that this is the case.

Table 6. MINIMUF-3 rms error versus geomagnetic latitude.

Geomagnetic Latitude	Sample, Path Months	% of Sample	rms Error, MHz
25°S to 25°N (transequatorial)	87	44	4.32
20°N to 60°N (midlatitude)	107	55	3.44
Greater than 60°N (polar)	2	1	3.18

For polar regions, the data available were insufficient to be conclusive. Furthermore, there were no data from the southern polar regions, which probably would have been quite different than the north polar region propagation. The most surprising aspect of table 6 is the success MINIMUF had with transequatorial paths. The variability of the F-region and the continuous E-region intervention around the equator make those regions difficult to predict. As seen in table 6, MINIMUF-3 does quite well with these types of paths, and the data sample is sufficient to be conclusive.

7. SOLAR SUNSPOT NUMBER (SSN)

A major consideration in MUF prediction is the ability of the model to deal with different phases of the solar sunspot cycle. Ideally, it should produce consistent results for SSN values between 1 and 150. In the acquisition of data for the MINIMUF-3 verification, care was exercised to assure that a sufficient cross section of sunspot numbers existed. Table 7 summarizes MINIMUF-3 performance as a function of SSN.

Table 7. MINIMUF-3 rms error versus solar sunspot number.

Sunspot Number (Cycle Phase)		Sample, Path Months	% of Sample	rms Error, MHz
10-30	(minimum)	73	37	3.20
31-60	(rise and decline)	11	6	4.15
61-90	(near maximum)	23	12	3.34
91-120	(maximum)	87	44	4.34
121-150	(high maximum)	2	1	4.63

Table 7 indicates that MINIMUF-3 accuracy declines somewhat at the solar maximum period.

The two path months of data taken near high maximum (ie, 1960; cycle 19) are suspect because available sounder instrumentation was extremely limited in that period. The remaining results are consistent with theory. As the solar cycle approaches maximum, the level of day-to-day activity increases. Compared to solar minimum conditions, solar maximum day-to-day variability in emission and resultant ionospheric support at higher frequencies is larger and more difficult to represent by mean values. This can be best illustrated by looking at the distribution of daily MOFs used to generate a mean MOF for a given hour. Figure 7 shows the MOF histogram for the Honolulu, Hawaii, to Corona, California, path at 1800 UT for the month of December 1968. The mean MOF is 27.3 MHz and the rms error in the observed MOF is 3.11 MHz. From the manner in which the daily MOFs are typically distributed, as shown in fig 7, it is expected that simple empirical models such as MINIMUF-3 will become less accurate at solar maximum because ambient conditions are more difficult to typify.

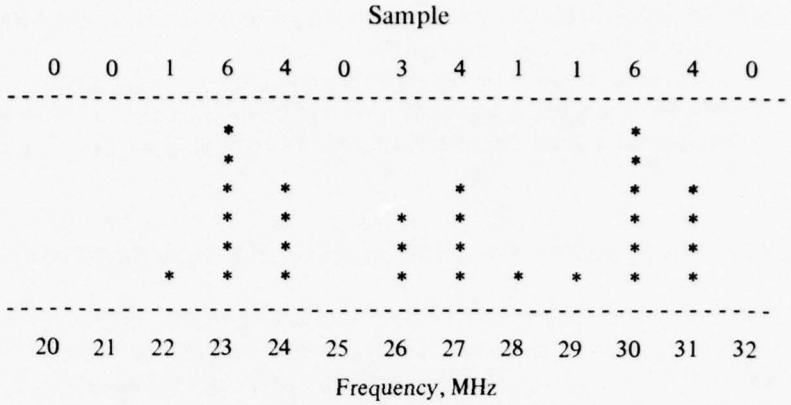

Figure 7. Distribution of daily MOFs (Honolulu, HI, to Corona, CA, December 1968 – 1800 UT – SSN = 98).

8. DIURNAL TRENDS

The last, and probably the most important, test of the MINIMUF-3 model involved the study of rms error as a function of time. The objective was to assure that the model could track through all aspects of the day/night cycle. To do this, the entire data set was converted to local path time (LPT); ie, the local time of the path midpoint. This put all the day, night, and transition characteristics in the same frame of reference. Figure 8 shows a plot of rms error as a function of LPT. The rms error varies between 3.25 MHz (0400 LPT) and 4.6 MHz (1800 LPT). The daylight error remains a nearly constant 3.9 MHz, with the greatest variation occurrring at night.

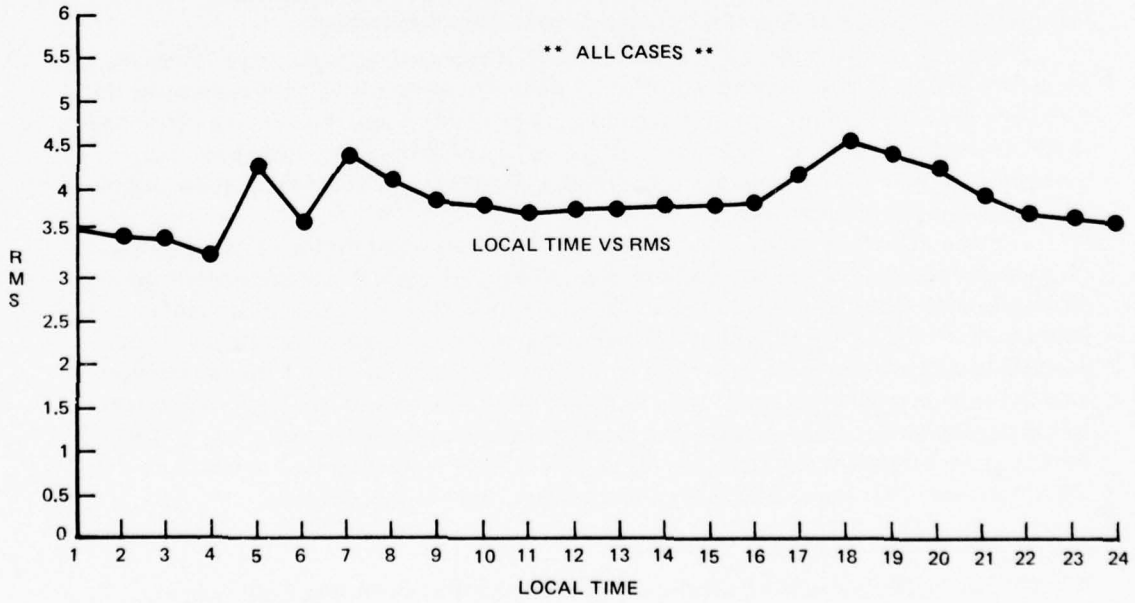

Figure 8. MINIMUF-3 Rms error as a function of local path time.

The source of the error seen in the period between 1800 and 2400 LPT is the post sunset lag in the MUF decay. This phenomenon is seen on most east-west midlatitude paths and is a dominant feature of transequatorial paths.

It is most difficult to model such characteristics because they are driven by ionospheric transport processes which are too complex for a simplified model such as MINIMUF-3 However, the model does do a good job of tracking the systematic changes which vary the day/night MUF.

COMPARISON BETWEEN MINIMUF-3 AND LARGE-SCALE hf PREDICTION CODES

Once the baseline accuracy of MINIMUF-3 was determined to be 3.83 MHz rms error, the next question to be resolved was, "How does this compare to other hf MUF prediction techniques?" This was a relatively straightforward task to undertake because of a previous study performed at NOSC. In this study (ref 17) three hf prediction large-scale computer codes (LSCC) were compared against oblique sounder data. Because many of the sounder data used were also part of the MINIMUF-3 verification data base, side-by-side comparisons could be made. All that was required was to rerun MINIMUF-3 against only that sounder information used in the earlier study.

The three LSCC programs reviewed were ESSA-ITSA-1 (ref 3), which is the basis for the Navy's NTP-6, and two versions of ITS-78 (ref 2) designated the "red deck" and "blue deck". These programs are quite extensive and predict a variety of other propagation parameters needed by system designers and engineers. Because of their complexity, they require a full-size computer (eg, IBM-370, UNIVAC 1110, etc) to perform the calculations.

To provide the side-by-side comparison between MINIMUF-3 and the three large-scale programs, a common oblique sounder data base was identified. Then MINIMUF-3 and the three large-scale programs were analyzed in the same manner presented in section B. The result is compiled in table 8 and is based on 137 path months of oblique sounder data. The data contain none of the high-quality NTSS-HFDR data, as the earlier study was performed before this digitized sounder information was available.

Overall, table 8 indicates that MINIMUF-3 is comparable to the larger programs in predicting MUF. For all cases tested, there is really very little to choose from among the four programs. In addition, the comparison shown in table 8 also reinforces a point made in the earlier study (ref 17). This was that, for any given propagation situation, one computer program will be superior to the others. However, for all situations, no program will be superior in all categories.

From table 8, it appears that MINIMUF-3 performs best during uncomplicated propagation conditions. When geophysical conditions arise which add complexity to the propagation picture, the larger programs are generally better. This is as it should be because MINIMUF-3 is a simplified estimation and is not designed to handle every conceivable situation. The most important point is that throughout table 8, the differences among the four prediction programs in each category are really insignificant with respect to solving day-to-day hf problems. The most obvious conclusion from this test is that, for any given propagation situation, a MINIMUF-3 MUF prediction is as likely to be correct as one of the large-scale prediction programs used in this analysis.

---

17. Sailors, DB, HF Propagation Predictions: Program Proliferation in the Real World, paper presented at NSA, 13 November 1973.

Table 8. Comparison of Large-Scale hf Prediction Codes and MINIMUF-3

Case Tested	Number of Path Months	RMS Residual Error (MHz)			
		MINIMUF-3	ESSA-ITSA-1	ITS-78 "Red"	ITS-78 "Blue"
All cases	137	4.03	5.2	4.6	4.5
Path length < 4000 km	31	4.41	5.7	6.3	6.5
Path length > 4000 km	106	3.88	4.1	4.1	3.6
$4000 \leqslant$ path length $\leqslant 5000$ km	53	3.88	5.4	4.2	3.7
Path length > 5000 km	47	3.88	4.0	3.9	3.5
$25^{\circ}S <$ geographic latitude $< 25^{\circ}N$	59	4.59	3.8	3.4	3.8
$20^{\circ}N <$ geographic latitude $< 60^{\circ}N$	76	3.65	5.4	5.2	4.9
Geographic latitude $> 60^{\circ}N$	2	3.18	6.7	4.8	4.9
SSN < 50	24	3.39	4.8	4.1	4.1
$50 <$ SSN < 100	58	4.01	5.6	5.3	5.0
SSN > 100	55	4.30	4.7	4.2	3.9
Winter months	27	3.64	4.7	5.6	5.1
Spring months	34	4.08	5.4	4.4	4.4
Summer months	42	3.92	5.4	3.4	3.5
Fall months	34	4.40	4.8	5.3	5.7

DISCUSSION OF RESULTS

Overall, the tests indicate that MINIMUF-3 produces a reasonably consistent product with a nominal accuracy between 3 and 5 MHz rms residual error. Except for certain transauroral cases, the model appears able to handle a variety of propagation situations without being overly sensitive to any particular parameter.

The purpose of this report is to provide the reader with a new propagation prediction tool and with enough information so that he can confidently use it.

The reader should also note that there are geographical areas not covered in this study because of the lack of readily available sounder data. Except for the paths terminating in HEH, Australia, the southern hemisphere is almost totally excluded. Transatlantic and Asian land mass data are also lacking. It is hoped that as new data become available, these areas can be checked and the results reported.

APPLICATIONS

MINIMUF-3 was designed to provide a quick estimate of MUF between any two geographical points for a variety of cases, using simple computational tools. It was not designed to replace the large-scale hf prediction codes in situations where the computer

facilities exist. MINIMUF's primary advantage lies with mobile propagation forecast requirements where the transmission path is continuously changing and limited computer facilities exist. It is these types of application that will be briefly discussed.

All users of the hf spectrum are concerned about whether a transmission made at a given frequency will be heard at some specified distant point. If the operating frequency is in the propagation bandwidth between the LUF and MUF, then the transmission should be heard. If not, some adjustment in frequency must be made. The primary problem is rapid identification of the MUF and LUF boundaries. A simplified method to calculate LUF has existed at NOSC for several years and has proven to be quite satisfactory. MINIMUF-3 provides an estimate of the upper MUF boundary which allows a complete definition of the propagation bandwidth for any given transmission path.

To illustrate how the model could be used, sample outputs from a mobile propagation forecast (PROPHET) system being developed around a Tektronix 4051 desk top graphics calculator were generated. Assume that a transmitter in Washington, DC, wishes to know his propagation coverage to London, Paris, Madrid, Rome, Tel Aviv, Capetown, Omaha, San Diego, Honolulu, Bogota, and Rio de Janeiro on 16.8 MHz. Figure 9 (a–d) shows which of these receivers can hear the transmission at 0, 6, 12, and 18 hours Universal Time (UT). Figure 9a indicates that at 0/hour/UT, only those paths to San Diego, Honolulu, Bogota, and Rio are open on 16.8 MHz. The remaining stations are in the night sector and the MUF on each path has dropped below the operating frequency. At 06/hours/UT (fig 9b), none of the paths is open, since all are in darkness or presunrise. At 12/hours/UT, fig 9c shows a variety of propagation bandwidth configurations. All the stations to the east of Washington are in daylight, and the MUF is well above 16.8 MHz. On the long path to Capetown, the LUF has risen to above 16.8 MHz. Stations to the west of Washington are still in night darkness and the MUF has not started to rise. The South American receivers to the south are in a sunrise/early morning state. At 1800/hours/UT (fig 9d), all the paths except Omaha are in daylight and 16.8 MHz is a good frequency for broad geographical coverage.

While only four samples are shown in fig 9, the mobile PROPHET terminal just as easily could have produced 24 or 48 examples. If driven by a date/time clock, a display similar to fig 9 could be updated automatically at any desired interval. Manipulation of the transmitter/receiver configuration is also quite easy.

Simplified propagation forecasting, such as that shown in fig 9, has many implications in the use of the hf spectrum. The ability to put this capability in mobile platforms permits a continuous knowledge of where a transmission can or cannot propagate to, allows better use of available frequencies, and provides a basis to exploit propagation characteristics to advantage in tactical or covert communications. Because of the small size and simplicity of these hf forecast tools, it is also realistic to envision that a point-to-point hf prediction capability could be an integral part of future microprocessor-controlled tranmitters and/or receivers.

CONCLUSIONS

MINIMUF-3 is designed to complement existing large-scale hf propagation codes when computation resources are limited and large-scale codes are not feasible to execute. In such circumstances, MINIMUF-3 can be used to generate first-order estimates of MUF.

15 OCT 1977 0 UT
X-RAY FLUX = 1.00E-004 SUNSPOT # = 15
WASH. DC LAT = 39.00 LON = 76.00

RECEIVER	DIST	LUF	FOT	MUF
LONDON	5849	2.0	9.3	11.0
PARIS	6126	2.0	9.6	11.3
MADRID	5955	2.0	9.9	11.7
ROME	7167	2.0	10.1	11.9
TEL AVIV	9387	2.0	9.7	11.4
CAPETOWN	12764	2.0	13.6	15.9
OMAHA	1714	2.0	7.9	9.3
SAN DIEGO	3760	2.0	15.7	18.4
HONOLULU	7378	9.0	22.3	26.3
BOGOTA	3786	2.0	18.6	21.9
RIO	7556	2.0	17.2	20.3

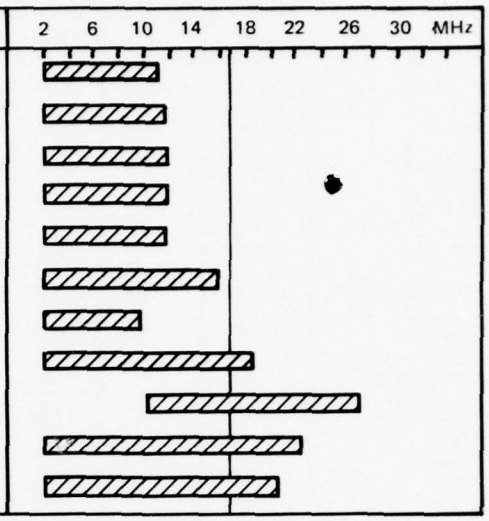

(a) 16.8 MHz

15 OCT 1977 600 UT
X-RAY FLUX = 1.00E-004 SUNSPOT # = 15
WASH. DC LAT = 39.00 LON = 76.00

RECEIVER	DIST	LUF	FOT	MUF
LONDON	5849	2.0	9.2	10.8
PARIS	6126	2.0	9.4	11.1
MADRID	5955	2.0	9.6	11.3
ROME	7167	2.0	10.0	11.7
TEL AVIV	9387	5.8	9.5	11.2
CAPETOWN	12764	7.6	11.1	13.1
OMAHA	1714	2.0	7.0	8.2
SAN DIEGO	3760	2.0	11.4	13.4
HONOLULU	7378	2.0	14.1	16.6
BOGOTA	3786	2.0	12.8	15.0
RIO	7556	2.0	12.4	14.6

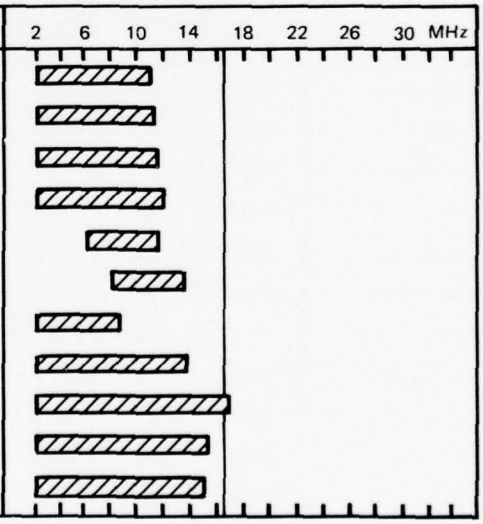

(b) 16.8 MHz

Figure 9. Application examples of MINIMUF-3.

15 OCT 1977 1200 UT
X-RAY FLUX = 1.00E-004 SUNSPOT # = 15
WASH. DC LAT = 39.00 LON = 76.00

RECEIVER	DIST	LUF	FOT	MUF
LONDON	5849	10.6	15.5	18.3
PARIS	6126	11.0	16.0	18.8
MADRID	5955	11.0	16.5	19.5
ROME	7167	12.2	17.2	20.2
TEL AVIV	9387	14.3	16.2	19.1
CAPETOWN	12764	17.8	18.6	21.9
OMAHA	1714	2.0	9.3	10.9
SAN DIEGO	3760	2.0	11.1	13.1
HONOLULU	7378	2.0	11.7	13.8
BOGOTA	3786	6.4	15.6	18.4
RIO	7556	11.8	17.8	20.9

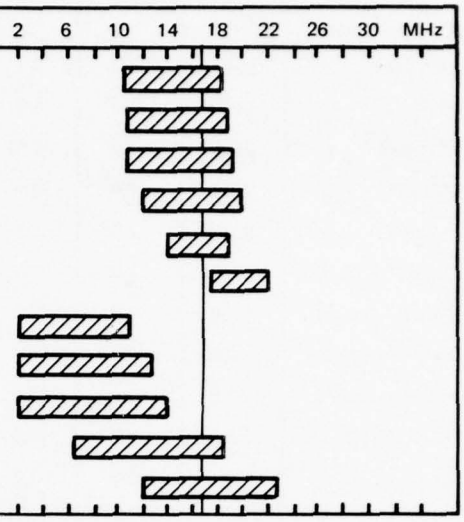

(c) 16.8 MHz

15 OCT 1977 1800 UT
X-RAY FLUX = 1.00E-004 SUNSPOT # = 15
WASH. DC LAT = 39.00 LON = 76.00

RECEIVER	DIST	LUF	FOT	MUF
LONDON	5849	9.1	16.9	19.9
PARIS	6126	9.1	17.3	20.3
MADRID	5955	9.3	17.8	21.0
ROME	7167	9.1	18.2	21.4
TEL AVIV	9387	8.4	17.5	20.5
CAPETOWN	12764	13.9	21.5	25.3
OMAHA	1714	6.6	13.5	15.9
SAN DIEGO	3760	10.6	21.9	25.7
HONOLULU	7378	13.3	21.0	24.7
BOGOTA	3786	10.5	23.6	27.7
RIO	7556	13.7	23.6	27.8

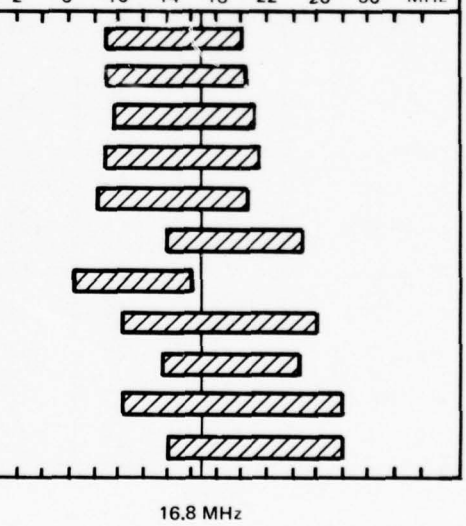

(d) 16.8 MHz

Figure 9. (Continued.)

Its intrinsic simplicity (80 BASIC or 90 FORTRAN statements) notwithstanding, the accuracy of MINIMUF-3, as judged by rms residuals when compared to hf oblique sounder data, is comparable to that of existing large-scale codes. For example, using a common data base consisting of 137 path months of nondigitized sounder data, MINIMUF-3 had an rms residual error of 4.0 MHz, which can be compared to the best (4.5 MHz for ITS-78 "blue deck") and the worst (5.2 MHz for ESSA-ITSA-1) errors experienced with the large-scale codes. When MINIMUF-3 was tested against 59 path months of high-quality digitized (NTSS–HFDR) data, the RMS residual error was 3.31 MHz. Overall, from a total data base of 196 path months of data from 23 different hf sounder paths, residual errors were distributed as shown in table 9.

Table 9. Distribution of MINIMUF-3 Errors

MINIMUF rms Residual Error	% of Total Sample
Less than 3.0 MHz	38
3.1 to 4.0 MHz	23
4.1 to 5.0 MHz	28
5.1 to 6.0 MHz	11

For all cases, the residual error was 3.83 MHz.

For all paths, MINIMUF-3 showed no significant bias errors as a function of the local time of the path control points, which indicates that diurnal effects are being properly modeled in an average sense.

When compared by means of a common data base, MINIMUF-3 outperformed all large-scale hf codes on transmission paths of less than 4000 km. Although this may be an artifact of the data base, it does indicate that f_0F_2 is probably being modeled better than the M factor. This is what one would expect, considering the overly simple M factor model employed in MINIMUF-3. (It also suggests that refinements of MINIMUF-3 should begin with refinements in the M-factor algorithms.)

From the overall data base, MINIMUF-3 accuracy shows no significant dependence on latitude, orientation, or seasonal factors. It will degrade slightly at high sunspot numbers (ie, SSN $\approx$ 100 expected in the 1980–1982 time frame) when day-to-day ionospheric variability is high because of solar activity. MINIMUF-3 accounts only for F-region propagation and its predictions will degrade in the presence of mixed modes caused by sporadic E* or when the E-layer itself dominates.

MINIMUF-3 is based on the simple idea that f_0F_2 can be modeled to a first approximation as the lagged response to a driving function proportional to $(\cos \chi)^n$ where χ is the instantaneous solar zenith angle and where the daytime lag is quite seasonally dependent. The general success of MINIMUF-3 over a broad range of hf transmission path conditions lends some credence to these ideas. However, consistent deviations from single exponential decays at night indicate that more complex relaxation processes are involved and will be reviewed as future refinements.

It is concluded that MINIMUF-3 is sufficiently accurate to provide a simplified prediction of hf maximum usable frequency (MUF) suitable for use on small mobile propagation forecast (PROPHET) terminals. With its inherent simplicity, it is fully expected

---

* Because of the well localized height of sporadic E reflections, it is a relatively straightforward problem to extend MINIMUF-3 to generate MUF forecasts for a variety of mixed-mode structures.

that other investigators will refine and improve the model presented here. It is hoped that the successes along this line will be openly reported so that the hf community as a whole can benefit.

RECOMMENDATIONS

It is recommended that work continue to further refine the MINIMUF-3 model to include E and sporadic E region propagation. With the acceptance of simplified propagation models, on-site, real-time propagation forecasting on a system-by-system basis becomes realistic and cost effective. It is recommended that a microprocessor-based propagation forecast (PROPHET) capability be considered as an integral part of new hf system development. Further, it is recommended that work continue in developing applications for the new hf prediction capabilities resulting from the availability of simplified models such as MINIMUF-3.

REFERENCES

1. International Radio Consultative Committee, 13th Plenary Assembly, Geneva 1974, Recommendation 373-3; Definitions of Maximum Transmission Frequencies, International Telecommunications Union, 1975.

2. Bennington, TW, How Many MUFs?, Wireless World, v 65, p 537–538, December 1959.

3. Richter, Dr JH, IJ Rothmuller, and RB Rose, PROPHET: Real Time Propagation Forecasting Terminal, paper presented at 7th Technical Exchange Conference, El Paso, Texas, 30 November 1976.

4. Environmental Sciences Services Administration technical report ERL-110-ITS-78, Predicting Long Term Operational Parameters of High Frequency Sky Wave Telecommunication Systems, by AF Barghausen, JW Finney, LL Proctor, and LD Schultz, May 1969.

5. Environmental Sciences Services Administration technical report IER-1-ITSA-1, Predicting Statistical Performance Indexes for High Frequency Ionospheric Telecommunication Systems, by DL Lucas, GW Haydon, et al, August 1966.

6. Stanford Research Institute, technical summary report no 7, Long Range Propagation Experiment, ONR contract no 3853(00), ARPA order 196–62, November 1964.

7. Booz, Allen, An Examination of the Data Presently Available for the Development of a Short-term Warning Capability, Applied Research Inc, report 800-9-5, prepared under contract no 93296, project serial no SS-267-001, task 7645, 23 February 1966.

8. Chief of Naval Operations (OEG) letter report, Data for Comparison of Ionospheric Sounder Measurements with Predicted Optimum Frequencies for Communication Circuits, letter serial (OEG) 154-70, 12 March 1970.

9. General Electric Co, Expanded Little Ida, Experimental Results, technical report no RADC-TR-67-618, prepared under contract AF30(602)-3946 for Rome Air Development Center, December 1967.

10. Stanford Research Institute, interim technical report 4, HF Communications Effects Simulation: Comparison of the Fort Monmouth/Palo Alto Circuit Performance with Computer Predictions, Army contract DA-36-039, SC-87197, DASA subtask 938/04-014, January 1964.

11. US Department of Commerce, Boulder–Barrow Sweep Frequency Oblique Pulse Experiment, NBS report 7217 by LH Tveten, 8 January 1962.

12. JA Ratcliffe and K Weekes, in Physics of the Upper Atmosphere, JA Ratcliffe (ed), p 427–432, Academic Press, New York, 1960.

13. Rishbeth, H, A Review of Ionospheric F Region Theory, Proc IEEE, v 55, p 16–35, January 1967.

14. International Radio Consultative Committee, Oslo, 1966, Report 340; CCIR Atlas of Ionospheric Characteristics, International Telecommunications Union, Geneva, 1975.

15. International Radio Consultative Committee, New Delhi, 1974, Supplement No 1 to Report 340; CCIR Atlas of Ionospheric Characteristics, International Telecommunications Union, Geneva, 1971.

16. International Radio Consultative Committee, Geneva, 1974, Supplement No 2 to Report 340; CCIR Atlas of Ionospheric Characteristics, International Telecommunications Union, Geneva, 1975.

17. Sailors, DB, HF Propagation Predictions: Program Proliferation in the Real World, paper presented at NSA, 13 November 1973.

APPENDIX A:

BASIC PROGRAM FOR MINIMUF-3

Input variables for MINIMUF-3 BASIC program:

L1 – TRANSMITTER LATITUDE, radians $\left(-\frac{\pi}{2} \leqslant L1 \leqslant \frac{\pi}{2}\right)$

W1 – TRANSMITTER WEST LONGITUDE, radians $(-2\pi \leqslant W1 \leqslant 2\pi)$

L2 – RECEIVER LATITUDE, radians $\left(-\frac{\pi}{2} \leqslant L2 \leqslant \frac{\pi}{2}\right)$

W2 – RECEIVER WEST LONGITUDE, radians $(-2\pi \leqslant W2 \leqslant 2\pi)$

MØ – MONTH $(1 \leqslant M\emptyset \leqslant 12)$

D6 – DAY $(1 \leqslant D6 \leqslant 31)$

T5 – TIME (UT), hours $(\emptyset.\emptyset \leqslant T5 \leqslant 24.0)$

J9 – OUTPUT MUF, MHz

S8 – SUNSPOT COEFFICIENT (250)

S9 – SUNSPOT NUMBER

PI – 3.141593

PØ – 1.570796

```
600 REM : MINI MUF II MOD 3   ********************************************
605 H3=1.59
610 K7=SIN(L1)*SIN(L2)+COS(L1)*COS(L2)*COS(W2-W1)
620 G1=ATN(SQR(1-K7*K7)/K7)+P0*(1-SGN(K7))
630 K6=H3*G1
635 IF K6=>1 THEN 640
636 K6=1
640 K5=1/K6
650 J9=100
660 FOR K1=1/(2*K6) TO 1-1/(2*K6) STEP 0.9999-K5
665 IF K5=1 THEN 670
666 K5=0.5
670 IF W1=>W2 AND W1-W2<PI THEN 730
680 IF W2>W1 AND W2-W1>PI THEN 730
690 W0=W1
700 A=P0-L1
710 C=P0-L2
720 GO TO 760
730 A=P0-L2
740 C=P0-L1
750 W0=W2
760 B=G1
770 GOSUB 1500
780 C=D
790 B=K1*G1
800 GOSUB 1470
810 C=B
820 B=D
830 GOSUB 1500
840 W0=W0+D
850 L0=P0-B
860 Y1=0.0172*(10+(M0-1)*30.4+D6)
870 Y2=0.409*COS(Y1)
880 K8=3.82*W0+12+0.13*(SIN(Y1)+1.2*SIN(2*Y1))
890 K8=K8-12*(1+SGN(K8-24))*SGN(ABS(K8-24))
891 IF COS(L0+Y2)>-0.26 THEN 900
896 G0=0
897 M9=SIN(2.5*G1*K5)
898 M9=1+2.5*M9*SQR(M9)
899 GO TO 1215
900 K9=(-0.26+SIN(Y2)*SIN(L0))/(COS(Y2)*COS(L0)+1.0E-3)
910 K9=12-ATN(K9/SQR(ABS(1-K9*K9)))*24/PI
920 T=K8-K9/2+12*(1-SGN(K8-K9/2))*SGN(ABS(K8-K9/2))
930 T4=K8+K9/2-12*(1+SGN(K8+K9/2-24))*SGN(ABS(K8+K9/2-24))
940 C0=ABS(COS(L0+Y2))
980 T9=9.7*C0↑9.6
985 IF T9>0.1 THEN 990
988 T9=0.1
990 M9=SIN(2.5*G1*K5)
1000 M9=1+2.5*M9*SQR(M9)
1030 IF T4<T THEN 1060
1040 IF (T5-T)*(T4-T5)>0 THEN 1070
1050 GO TO 1240
1060 IF (T5-T4)*(T-T5)>0 THEN 1240
1070 T6=T5+12*(1+SGN(T-T5))*SGN(ABS(T-T5))
1090 G9=PI*(T6-T)/K9
1100 G8=PI*T9/K9
1110 U=(T-T6)/T9
1190 G0=C0*(SIN(G9)+G8*(EXP(U)-COS(G9)))/(1+G8*G8)
1195 G3=C0*(G8*(EXP(-K9/T9)+1))*EXP((K9-24)/2)/(1+G8*G8)
1200 IF G0=>G3 THEN 1215
1210 G0=G3
1215 G2=(1+S9/S8)*M9*SQR(6+58*SQR(G0))
1220 G2=G2*(1-0.1*EXP((K9-24)/3))
1225 G2=G2*(1+(1-SGN(L1)*SGN(L2))*0.1)
1226 G2=G2*(1-0.1*(1+SGN(ABS(SIN(L0))-COS(L0))))
1230 GO TO 1430
1240 T6=T5+12*(1+SGN(T4-T5))*SGN(ABS(T4-T5))
1250 G8=PI*T9/K9
```

```
1260 U=(T4-T6)/2
1330 U1=-K9/T9
1400 G0=C0*(G8*(EXP(U1)+1))*EXP(U)/(1+G8*G8)
1420 GO TO 1215
1430 IF G2>J9 THEN 1450
1440 J9=G2
1450 NEXT K1
1460 RETURN
1470 REM *** COSLAW ***
1480 D=ACS(COS(A)*COS(B)+SIN(A)*SIN(B)*COS(C))
1490 RETURN
1500 REM *** TANLAW ***
1510 S=(A+B+C)/2
1520 IF C>1.0E-5 AND ABS(C-ABS(A-B))>1.0E-5 THEN 1550
1530 D=0
1540 RETURN
1550 IF ABS(S-C)>1.0E-5 THEN 1580
1560 D=PI
1570 RETURN
1580 D=2*ATN(SQR(SIN(S-A)*SIN(S-B)/(SIN(S-C)*SIN(S))))
1590 RETURN
```

APPENDIX B:

FORTRAN PROGRAM FOR MINIMUF-3

Input variables for MINIMUF-3 FORTRAN:

W – TRANSMITTER LATITUDE, radians $\left(-\frac{\pi}{2} \leqslant W \leqslant \frac{\pi}{2}\right)$

X – TRANSMITTER WEST LONGITUDE, radians $(-2\pi \leqslant X \leqslant 2\pi)$

Y – RECEIVER LATITUDE, radians $\left(-\frac{\pi}{2} \leqslant Y \leqslant \frac{\pi}{2}\right)$

Z – RECEIVER WEST LONGITUDE, radians $(-2\pi \leqslant Z \leqslant 2\pi)$

M – MONTH $(1 \leqslant M \leqslant 12)$

D – DAY $(1 \leqslant D \leqslant 31)$

T5 – TIME (UT), hours $(\emptyset.\emptyset \leqslant T5 \leqslant 24.\emptyset)$

J9 – CMUF – OUTPUT MUF, MHz

S8 – SUNSPOT COEFFICIENT (250)

S9 – SUNSPOT NUMBER

```
      SUBROUTINE MUFII( W, X, Y, Z, M, D, T5, J9, S8, S9 )
C
C
      LOGICAL         SGN
C
C
      REAL            K7, K5, L0, K8, K9, J9, M9
      REAL            SAVE(24)
C
      COMMON          /BROCK/   SAVE
      DATA            PI /3.141593/, P0 /1.570796/, P1 /6.283185/,
     #                DEG /57.29578/
C
      K7=SIN(W)*SIN(Y)+COS(W)*COS(Y)*COS(Z-X)
      G1 = ARCOS( K7 )
      H3 = 1.59
      AK6 = H3 * G1
      IF ( AK6 .LT. 1.0 ) AK6 = 1.0
      KHOP = 1
      IF ( AK6 .GT. 1.0 ) KHOP = 2
      K5=1.0/AK6
        IF ( K5 .NE. 1.0 ) K5 = 0.5
      J9=100.0
      DO 820 K1=1,KHOP
      AK1=1.0/(2.0*AK6)+FLOAT(K1-1)*( 0.9999 - 1.0/AK6 )
      SGN = Z .GE. X .AND. Z - X .LT. PI .OR.
     #      X .GT. Z .AND. X - Z .GT. PI
      IF ( .NOT. SGN )  GO TO 100
      A = PO - W
      B = PO - Y
      WO = X
      GO TO 120
  100 CONTINUE
      A = PO - Y
      B = PO - W
      WO = Z
  120 CONTINUE
      ALPHA = TANLAW( A, G1, B )
      B = AK1*G1
      LO = ARCOS( COS( A )*COS( B ) + SIN( A )*SIN( B )*COS( ALPHA ) )
      DELTA = TANLAW( A, LO, B )
      LO = PO - LO
      WO = WO + DELTA
      IF ( WO .GT. P1 )  WO = WO - P1
  260 Y1=0.0172*(10.0*FLOAT(M-1)*30.4+D)
```

```
190         Y2=0.409*COS(Y1)
191         K8=3.82*W0+12.0+0.13*(SIN(Y1)+1.2*SIN(2.0*Y1))
192   290   K8 = K8 - 12.0*(1.0 + SIGN( K8 - 24.0))*SIGN( ABS( K8 - 24.0 ) )
193           IF ( COS( L0 + Y2 ) .GT. -0.26 )  G0 TO 300
194         G0 = 0.0
195         M9 = SIN( 2.5*G1*K5 )
196         M9 = 1.0 + 2.5*M9*SQRT( M9 )
197         G0 TO 590
198   300   K9 = ( -0.26 + SIN( Y2 )*SIN( L0 ) )/( COS( Y2 )*COS( L0 ) +
199        #         1.0E-3 )
200         K9 = 12.0 - ATAN( K9/SQRT( ABS( 1.0 - K9*K9 ) ) )*7.6394
201   310   T=K8-K9/2.0+12.0*(1.0-SIGN(K8-K9/2.0))*SIGN(ABS(K8-K9/2.0))
202   330   T4=K8+K9/2.0-12.0*(1.0+SIGN(K8+K9/2.0-24.0))*
203        #  SIGN(ABS(K8+K9/2.0-24.0))
204         C0 = ABS( COS( L0 + Y2 ) )
205   360   T9=9.7*C0**9.6
206         IF ( T9 .LT. 0.1 )  T9 = 0.1
207   370   M9=SIN(2.5*G1*K5)
208         M9=1.0+2.5*M9*SQRT(M9)
209   410   IF (T4.LT.T) G0TO 440
210         IF( (T5-T)*(T4-T5) .GT. 0.0 )  G0 TO 450
211         G0 TO 610
212   440   IF( (T5-T4)*(T-T5) .GT. 0.0 )  G0 TO 610
213   450   T6 = T5+12.0*(1.0+SIGN(T-T5))*SIGN(ABS(T-T5))
214         G9=PI*(T6-T)/K9
215   470   G8=PI*T9/K9
216         U = ( T - T6 )/T9
217         U = AMIN1( U, 120.0 )
218         U = AMAX1( U, -120.0 )
219   560   G0=C0*(SIN(G9)+G8*(EXP(U)-COS(G9)))/(1.0+G8*G8)
220         G3=C0*(G8*(EXP(-K9/T9)+1.0))*EXP((K9-24.0)/2.0)/(1.0+G8*G8)
221         IF ( G0 .LT. G3 )  G0 = G3
222   590     G2 = ( 1.0 + S9/S8 )*M9*SQRT( 6.0 + 58.0*SQRT( G0 ) )
223           G2 = G2*( 1.0 - 0.1*EXP( ( K9 - 24.0 )/3.0 ) )
224           G2 = G2*( 1.0 + ( 1.0 - SIGN( W )*SIGN( Y ) )*0.1 )
225           G2 = G2*( 1.0 - 0.1*( 1.0 + SIGN( ABS( SIN( L0 ) ) - COS( L0))))
226         G0 TO 800
227   610   T6 = T5+12.0*(1.0+SIGN(T4-T5))*SIGN(ABS(T4-T5))
228         G8=PI*T9/K9
229         U=(T4-T6)/2.0
230         U = AMIN1( U, 120.0 )
231         U = AMAX1( U, -120.0 )
232         U1=-K9/T9
233         U1 = AMIN1( U1,  120.0 )
234         U1 = AMAX1( U1, -120.0 )
```

```
  235  770    G0=C0*(G8*(EXP(U1)+1.0))*EXP(U)/(1.0+G8*G8)
  236         G0 T0 590
  237  800    C0NTINUE
  238         IF(G2.GT.J9) G0 T0 815
  239  810    J9=G2
  240  815    C0NTINUE
  241         LQ = ( K1 - 1 )*7
  242         SAVE(LQ+1) = L0
  243         SAVE(LQ+2) = W0
  244         SAVE(LQ+3) = K8
  245         SAVE(LQ+4) = K9
  246         SAVE(LQ+5) = T
  247         SAVE(LQ+6) = T4
  248         SAVE(LQ+7) = C0
  249  820    C0NTINUE
  250         SAVE(15) = G1
  251         SAVE(16) = AK6
  252         SAVE(17) = K5
  253         SAVE(18) = Y1
  254         SAVE(19) = Y2
  255         SAVE(20) = D
  256         SAVE(21) = FL0AT(KH0P)
  257         SAVE(22) = FL0AT(M)
  258         SAVE(23) = S9
  259         SAVE(24) = SIGN( W )*SIGN( Y )
  260         SAVE(25) = SIGN( ABS( SIN( L0 ) ) - C0S( L0 ) )
  261  830    RETURN
  262         END
ERR0RS       0  SIZE  02447  START  00022
```

```
  263         FUNCTION TANLAW( A, B, C )
  264   C
  265   C           FOR A SPHERICAL TRIANGLE WITH SIDES A, B, C,
  266   C           TANLAW RETURNS THE ANGLE OPPOSITE C IN RADIANS
  267   C
  268         IF ( A + B .GE. C .AND.
  269        #     A + C .GE. B .AND.
  270        #     B + C .GE. A )  GO TO 120
  271         WRITE(4,100)  A, B, C
  272   100   FORMAT(/22HINVALID ARGS IN TANLAW,1P3E15.5/)
  273         RETURN
  274   120   IF ( C .GT. 1.0E-5 .AND. ABS( C - ABS( A - B ) ) .GT. 1.0E-5 )
  275        #          GO TO 140
  276         TANLAW = 0.0
  277         RETURN
  278   140   S = ( A + B + C )/2.0
  279         IF ( ABS( S - C ) .GT. 1.0E-5 )  GO TO 160
  280         TANLAW = 3.141593
  281         RETURN
  282   160   TANLAW = 2.0*ATAN( SQRT( SIN( S - A )*SIN( S - B )/
  283        #    ( SIN( S - C )*SIN( S ) ) ) )
  284         RETURN
  285         END
ERRORS       0  SIZE  00355  START  00003
```

```
  286          FUNCTION SIGN( Y )
  287    C
  288    C     ************************************************************************
  289    C     *
  290    C     *      PROGRAMMER:  BOB EVERHARDT, SDSUF
  291    C     *
  292    C     *      PURPOSE:
  293    C     *            OBTAIN THE ALGEBRAIC SIGN OF THE ARGUMENT                  *
  294    C     *
  295    C     *      INPUT:
  296    C     *            Y = ANY REAL NUMBER                                        *
  297    C     *
  298    C     *      OUTPUT:
  299    C     *            SIGN = -1.0 IF Y < 0.0                                     *
  300    C     *            SIGN =  0.0 IF Y = 0.0                                     *
  301    C     *            SIGN = +1.0 IF Y > 0.0
  302    C     *
  303    C     *
  304    C     ************************************************************************
  305    C
  306          IF ( Y .LT. 0.0 )  SIGN = -1.0
  307          IF ( Y .EQ. 0.0 )  SIGN =  0.0
  308          IF ( Y .GT. 0.0 )  SIGN = +1.0
  309          RETURN
  310          END
ERRORS       0  SIZE  00073  START  00001
```

INITIAL DISTRIBUTION

NAVAL ELECTRONIC SYSTEMS COMMAND
PME106-3 (DG ROBBINS)
NELEX-00BE (W COOK)

NAVAL SECURITY GROUP COMMAND
NAVAL SECURITY GROUP HEADQUARTERS
G-53 (LT J FITTEN)

CHIEF OF NAVAL OPERATIONS
NOP-941F (HA FEIGLESON)

NAVY ELECTROMAGNETIC SPECTRUM CENTER
NAVAL COMMUNICATION UNIT, WASHINGTON
WASHINGTON, DC 20390
CAPT JA MADIGAN

INSTITUTE FOR TELECOMMUNICATION SCIENCES
BOULDER, CO 80302
DON LUCUS (3)

CENTER FOR NAVAL ANALYSIS
1401 WILSON BLVD
ARLINGTON, VA 22209
CDR L SHOUP (3)

MEGATEK CORPORATION
1055 SHAFTER STREET
SAN DIEGO, CA 92106
DR PH LEVINE

MITRE CORP
WESTGATE RESEARCH PARK
MC LEAN, VA 22101
DR ALLAN SCHNEIDER

GENERAL ELECTRIC CO
BLDG 4, ROOM 48, COURT STREET PLANT
SYRACUSE, NY 13201
DR GEORGE H MILLMAN

TRACOR, INC
1600 WILSON BLVD
ARLINGTON, VA 22209
DR THEODORE J COHEN

SOUTHWEST RESEARCH INSTITUTE
8500 CULEBRA ROAD
PO DRAWER 28510
SAN ANTONIO, TX 78284
WM SHERRILL

COMMUNICATIONS RESEARCH CENTER
SHIRLEY BAY, BOX 490, STATION A
OTTAWA, ONTARIO, K1N85S, CANADA
UI CAMPBELL

JOHNS HOPKINS UNIVERSITY
APPLIED PHYSICS LABORATORY
JOHNS HOPKINS ROAD
LAUREL, MD 20810
TOM EVANS

DEFENSE DOCUMENTATION CENTER (12)


LMED
78